Ref. Ares(2022)7255761 – 19/10/2022

Benchmark cases D2.1

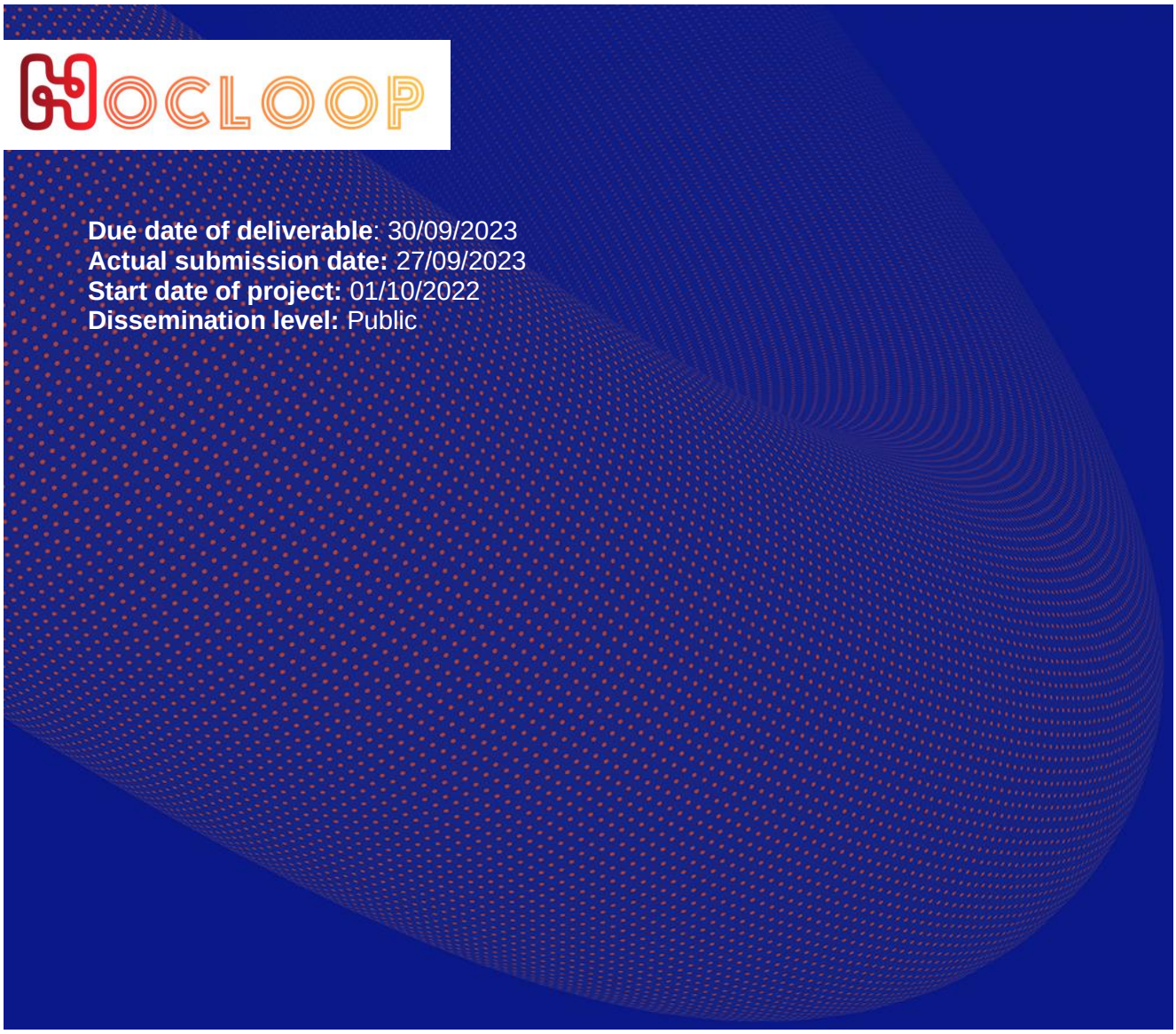

Due date of deliverable: 30/09/2023
Actual submission date: 27/09/2023
Start date of project: 01/10/2022
Dissemination level: Public

Funded by the European Union. Views and opinions expressed are however those of the author(s) only and do not necessarily reflect those of the European Union or CINEA. Neither the European Union nor the granting authority can be held responsible for them.

Prepared by	Reviewed Internally by	Reviewed Externally by	Approved by
Edgar Hernandez Acevedo (VITO) Vlasios Leontidis (IFPEN) Magnus Wangen (IFE) Virginie Harcouët-Menou (VITO)	Vlasios Leontidis (IFPEN) Virginie Harcouët-Menou (VITO) Mario Silva (IFE)	Ola Vestavik (RW) Domenico Liotta (UNIBA)	Mario Silva (IFE)

Technical References

Project Acronym	HOCLOOP
Project Title	A circular by design environmentally friendly geothermal energy solution based on a horizontal closed loop - HOCLOOP
Project Coordinator	IFE
Project Duration	42 months

Deliverable No.	D2.1
Dissemination level [1]	PU
Work Package	WP2
Task	2.1
Lead beneficiary	VITO
Contributing beneficiary(ies)	IFE, IFPEN
Prepared by /Author(s)	Edgar Hernandez Acevedo (VITO), Vlasios Leontidis (IFPEN) Magnus Wangen (IFE), Virginie Harcouët-Menou (VITO)
Reviewed by	Ola Vestavik (RW), Domenico Liotta (UNIBA)
Approved by/Coordinator	Mario Silva (IFE)
Due date of deliverable	30/09/2023
Actual submission date	27/09/2023

[1]PU = Public
PP = Restricted to other program participants (including the Commission Services)
RE = Restricted to a group specified by the consortium (including the Commission Services)
SE = Sensitive, only for members of the consortium (including the Commission Services)

Document history			
V	**Date**	**Author(s) /Reviewer(s) (Beneficiary)**	**Description (examples)**
0.1	01/05/2023	Edgar Hernandez Acevedo (VITO) Vlasios Leontidis (IFPEN) Magnus Wangen (IFE) Virginie Harcouët-Menou (VITO)	First Draft
0.2	01/06/2023	Edgar Hernandez Acevedo (VITO) Vlasios Leontidis (IFPEN) Magnus Wangen (IFE)	First internal revision

		Virginie Harcouët-Menou (VITO)	
0.3	01/08/2023	Virginie Harcouët-Menou (VITO) Vlasios Leontidis (IFPEN)	Second Internal
0.4	12/09/2023	Mario Silva (IFE)	Second draft Distributed
0.5	24/09/2023	Domenico Liotta (UNIBA) Ola Vestavik (RW)	Reviewer Comments
1.0	27/09/2023	Mario Silva (IFE)	Comments Addressed, Final version
2.0	27/09/2023	Mario Silva (IFE)	Document uploaded

Disclaimer

This document is partly based on the EC's official documents and profound knowledge of guidelines and ways of working in Horizon Europe. While guidelines on administration and reporting are as much as possible the same as the official documents, adjustments have been made with logical build-up and readability in mind. However, no legal responsibility can be taken for the contents in this document. If in doubt with an issue, please consult the official documents, or ask IFE, who will ask for an official EC response if necessary.

List of Abbreviations

EoS	Equation-of-State
GTW	Geo-Thermal-Well
GWellFM	Geothermal Well Flow Simulator

Table of Contents

List of Figures

List of Tables

Executive Summary Deliverable

Scope of the deliverable

The objective of WP2 is to develop tools and models to predict the heat flow towards a closed-loop geothermal well and the associated temperature decrease of the surrounding rock, considering the rock properties, groundwater flow and the different layers of the walls of the well, such as casing and cement. Within WP2, Task 2.1 aims at developing procedures for benchmarking geothermal simulators either commercial or in-house. The objective is to have a first stage validation of different software to be used in the modelling tasks of the project and in the design of the HOCLOOP concept.

Main conclusions

Analytical solutions to forecast the heat production from closed-loop geothermal systems in vertical and horizontal wells are available in the literature for symmetric rock domains with homogeneous properties in the radial direction and incompressible recirculation fluids. Additionally, in this deliverable an extension of Ramey's analytical solution to consider either heterogeneous rocks properties or horizontal wells is proposed.

The analytical solutions were used to benchmark the following numerical simulators: COMSOL (VITO), GWellFM (IFPEN) and GTW (IFE). The three simulators were able to reproduce the mentioned analytical solutions. Depending on their capabilities, these simulators can be used with confidence in more complex cases like the use of CO_2 as energy carrier fluid, well interference and effect of groundwater flow among others.

GWellFM and GTW simulators handle cylindrical discretization. This makes them suitable for modelling individual closed-loop geothermal wells. Nevertheless, this discretization can limit the modelling capabilities for problems that involve more than one well or wells with multiple branches.

Setting the simulation case for closed-loop geothermal wells is a straightforward task in GWellFM and GTW simulators while it is time-consuming in COMSOL. The numerical modelling challenge is the large number of cells required to model deep and long deviated wells in asymmetric 3D domains. This is because the whole domain from the surface to the bottom needs to be included. This can be overcome by verticalizing the well trajectories while acknowledging for changes in temperature gradient and rock properties.

The average variation between the results from the simulators modelling closed-loop cases was lower than 5%

The lack of field experiences and data with recorded temperature along deep well is the main limitation for the evaluation of the simulators and their assumptions.

1. Introduction

The objective of WP2 is to develop tools and models to predict the heat flow towards a closed-loop geothermal well and the associated temperature decrease of the surrounding rock, accounting rock properties, groundwater flow and the different elements of the well completion, such as casing and cement. Within WP2, T2.1 aims at developing procedures for benchmarking geothermal simulators either commercial or in-house. The objective is to have a first stage validation of different software to be used in the modelling tasks of the project and in the design of the HOCLOOP concept.

The benchmarking procedure considers 2 in-house simulators: GWellFM from IFPEN and GTW from IFE and the commercial simulator COMSOL (VITO). These simulators are benchmarked against single injection wells and closed-loop geothermal well problems that counts with analytical solutions. The accuracy and the ease for setting problems are aspects considered during the benchmark process. In addition, the effects of the circulation flow rate and inner tubing's thermal conductivity on temperature and power production are explored.

The report is divided as follows: The methodology chapter describes the analytical solutions for closed-loop geothermal wells, the evaluated simulators, and the benchmark cases. In addition, all input parameters, related with the benchmark cases, are detailed in this chapter. In the result section, a qualitative and quantitative evaluation of the simulators in terms of accuracy is shown. The discussion chapter explains the performance of the difference simulators and shows a comparison between them. Finally, the main findings are summarized in the conclusions.

2. Objectives

The deliverable contributes towards the following Work Package 2 objectives:

- Validate available numerical tools to simulate the HOCLOOP heat extraction concept and to understand the evolution of the rock temperature in the surrounding rock and the heat transport towards the well.
- Analyse the sensitivity of the heat production evolution through time to rock thermal properties, internal tubing thermal conductivity and operational flow rate.

This deliverable is a first of a series on the validation of the modelling approaches and tools that should be used when optimizing the design of the HOCLOOP solution and whole process considering the reservoir and the surface equipment.

3. Methodology

Procedures for benchmarking geothermal simulators were developed in task T2.1. First, the different simulators to be tested were selected. Then, a series of test cases for benchmarking the simulators were defined. Existing and new developed analytical solutions for the temperature in an injection well and the surrounding rock were used for software validation. The benchmarking of heat flow in the rock towards the well assumes an incompressible fluid in the well, in this case, water. Simulation results obtained using the different available simulation tools were compared for all cases to uncover the weaknesses and strengths of each tool.

3.1 Heat transfer equations

Fluid flow within the tubing (and annulus for coaxial wells) is considered steady state, single-phase, 1D in the vertical direction and incompressible, whereas the heat conduction through the formation surrounding the wellbore is considered unsteady and 2D in the radial and the vertical direction. Heat conduction through solids is generally expressed by the radial [1]:

$$\frac{1}{r}\frac{\partial}{\partial r}\left(r\frac{\partial T_e}{\partial r}\right)+\frac{\partial}{\partial z}\frac{\partial T_e}{\partial z}=\frac{1}{a_e}\frac{\partial T_e}{\partial t} \quad (1)$$

where T_e [°C] is the formation temperature and α_e [m^2/s] is the rock's thermal diffusivity.

The problem in defined by the below initial and boundary conditions:

$$t=0\ \&\ r\geq r_{cf}: T_e=T_e(z=0)+g_T z$$

$$t>0\ \&\ r=r_{cf}: Q=2\pi r_{cf}U\left(T_f-T_e\right)$$

$$t>0\ \&\ r=\infty: T_e=T_e(z=0)+g_T z$$

where z [m] is the position along the well in the flow direction (z = 0 is the well inlet), g_T [°C/m] is the geothermal gradient (positive for injection wells with z = 0 at the surface and negative for production wells with z = 0 at the bottom of the well), r_{cf} [m] is the outer diameter of the wellbore, Q [J/s/m] is the heat losses to the formation per length unit and U [W/m^2/K] is the overall heat transfer coefficient between the fluid and the wellbore (last layer before the rocks). A schematic representation of the domain describing the main geometrical parameters for a vertical closed well is shown in Figure 1.

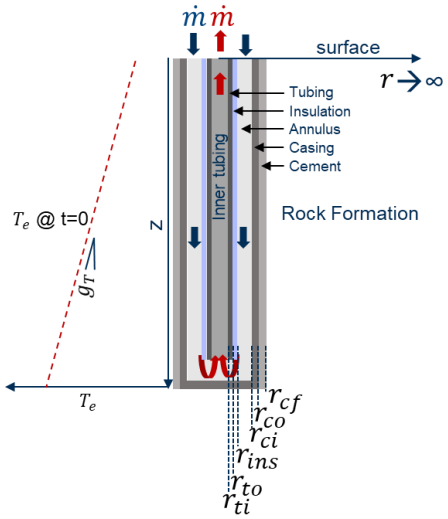

Figure 1. Description of the modelled domain and initial temperature condition for a closed-loop system in a vertical well.

The heat transfer coefficient between the inner tubing and the wellbore-formation interface (r_{cf}), considering a coaxial well with two fluids (fluid 1, fluid 2) and a sequence of other layers (tubing, insulation, casing and cement), can be expressed as:

$$U = \frac{1}{2\pi r_{cf} R_\theta} \tag{2}$$

where R_ϑ [m.K/W] is the total thermal resistance. The calculation of the overall thermal resistance is given by the below equation, and it can be modified according to the different materials that are present in the well completion.

$$R_\theta = \frac{1}{2\pi}\left[\frac{1}{r_{ti}h_{f_1}} + \frac{\ln\left(\frac{r_{to}}{r_{ti}}\right)}{k_t} + \frac{\ln\left(\frac{r_{ins}}{r_{to}}\right)}{k_{ins}} + \frac{1}{r_{ins}h_{f_2}} + \frac{\ln\left(\frac{r_{co}}{r_{ci}}\right)}{k_{cas}} + \frac{\ln\left(\frac{r_{cf}}{r_{co}}\right)}{k_{cem}}\right] \tag{3}$$

In the above equation, k [W/m/K] is material's conductivity, r [m] the corresponding radius and h_f [W/m^2/K] is fluid's forced convective heat transfer coefficient. The definition of the different radius is included on Figure 1.

For the forced convective heat transfer coefficient several equations can be found in the literature. All of them calculate the Nusselt number as a function of other non-dimensional numbers (Nusselt law). Here, the Dittus-Boelter model was applied:

$$Nu = 0.023 Re^{0.8} Pr^{0.4} \tag{4}$$

where the Nusselt, Reynolds and Prandtl numbers depend on the fluid physical properties (density, ρ [kg/m^3], viscosity, μ [Pa.s], thermal capacity, C_p [J/K/kg]) and fluid velocity, u [m/s]):

$$\begin{aligned} Re &= \frac{2r_{ti}u\rho_f}{\mu_f} \\ Nu &= \frac{h_f 2r_{ti}}{k_f} \\ Pr &= \frac{\mu_f C_{pf}}{k_f} \end{aligned} \tag{5}$$

The 1D energy balance (neglecting heat losses caused by friction) is governed by the below equation:

$$\frac{\partial}{\partial t}\left[A\rho_f\left(H + \frac{u^2}{2} - g\sin\theta\, z\right)\right] + \frac{\partial}{\partial z}\left[\dot{m}\rho_f\left(H + \frac{u^2}{2} - g\sin\theta\, z\right)\right] = -Q \tag{6}$$

where A [m^2] is the cross-section of the tubing, H [J/kg] is the specific enthalpy of the fluid, g [m/s^2] is the acceleration of gravity and Q [W/m] are the heat losses.

For incompressible fluids (like liquid water), the specific enthalpy is:

$$dH = C_{pf} dT_f + g\sin\theta\, dz \tag{7}$$

where T_f [°C] is the temperature of the fluid. Neglecting the kinetic energy, the resulting simplified energy balance is:

$$A\rho_f C_{pf}\frac{\partial T_f}{\partial t} + \dot{m}\rho_f Cp_f \frac{\partial T_f}{\partial z} = -Q \tag{8}$$

For steady-state heat flow in the well, the above equation can be further simplified by neglecting the temporal term on the left side.

3.2 Analytical tools

Ramey's analytical solution

Ramey [2] presented an analytical model to predict the heat loss between wellbore and formation in liquid and gas injection wells. In his model, the heat flow in the wellbore is considered much faster than that in the formation. Thus, the heat transfer process in the wellbore is approximated by a steady-state heat flow. On the other hand, the heat transmission in the formation around the wellbore is an unsteady-state process. Thus, it is only valid at long time scales (the thermal diffusion length must be significantly larger than the well radius or the fluid convection time scale must be significantly smaller than the conduction time scale). A time function is used to describe the diffusion of heat from the outer wellbore radius to the infinite formation boundary.

To derive the solution for liquid flow, Ramey assumed constant fluid and rock properties, no phase change in the well, non-compressible flow and zero friction and kinetic energy. Ramey's solution for the fluid temperature in a well as a function of time and position is:

$$T_f(z,t) = T_e(z=0) + g_T z - g_T \Lambda + [T_o + g_T \Lambda - T_e(z=0)] e^{-\frac{z}{\Lambda}} \quad (9)$$

where T_o [°C] is the fluid at the well inlet and Λ [m] is a function given by the equation:

$$\Lambda = \frac{\dot{m} C_{pf} (k_e + r_{ti} U f_t)}{2\pi r_{ti} U k_e} \quad (10)$$

where k_e [W/m/K] is rock's thermal conductivity, r_{ti} [m] is the inner radius of the well (inner tubing) and f_t is a characteristic time function describing the transient heat conduction in the host rocks. For an infinite constant heat flux the time function (for long times) is:

$$f_t = -\ln\left(\frac{r_{cf}}{\sqrt{4 a_e t}}\right) - 0.29 \quad (11)$$

where t [s] is the time.

An important note is that when simulations are performed for coaxial wells with a fluid circulating in the annulus and the central tubing parts, the Ramey solution can be applied only for the annulus fluid considering the heat exchange with the formation but not the heat interaction between the two fluids.

Modified Ramey's analytical solution

Approximated analytical solutions for vertical and horizontal wellbores with different lithologies and/or different geothermal gradients were developed during this project. It consisted in looping Ramey's solution one after the other for every domain (lithology or change in well trajectory). Thus, the temperature within every domain k can be computed with the next equation:

$$T_{f,k}(z,t) = T_e(z=0) + \sum_{k=1,k>1}^{k-1} g_{T,k} Z_k + g_{T,k}(z - Z_{k-1}) - g_{T,k} \Lambda_k + C_k e^{-\frac{z - Z_{k-1}}{\Lambda_k}} \quad (12)$$

where Z_{k-1} is the depth of the upper border of the domain k and C a characteristic constant:

$$C_k = \left[T_f(z = Z_{k-1}, t) - T_e(z=0) - \sum_{k=1,k>1}^{k-1} g_{T,k} Z_k + g_{T,k} \Lambda_k \right] \quad (13)$$

The development of this equation is given at Annex A1.

For instance, to apply Eq. (12) to a horizontal well drilled in a homogeneous media, the well is assumed or idealized vertical as shown in Figure 2 (right). This action generates two domains with different

temperature gradients: the vertical gradient and the horizontal gradient with a value of zero for the latter (constant temperature). Then, the wellbore temperatures in these two domains are computed following Eq. (12).

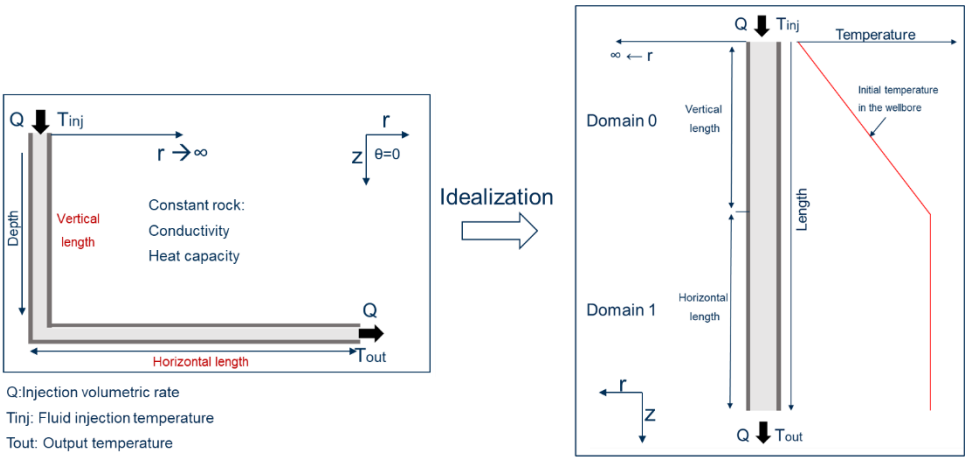

Figure 2. Horizontal well sketch (left) and corresponding idealization (right) for applying Ramey's modified analytical solution.

Kabir's analytical solutions

Hasan & Kabir [3] proposed a modification of Ramey's time function applicable for short and long times:

$$f_t = \begin{cases} 1.1281\sqrt{t_D}\left(1-0.3\sqrt{t_D}\right), & 10^{-10} \le t_D \le 1.5 \\ (0.4063+0.5\ln t_D)\left(1+\dfrac{0.6}{t_D}\right), & t_D > 1.5 \end{cases} \tag{14}$$

where t_D is the dimensionless time given as:

$$t_D = \frac{k_e t}{C_{pe}\rho_e r_{cf}^2} \tag{15}$$

In the above equation, C_{pe} [J/kg-K] and ρ_e [kg/m^3] are the heat capacity and density of the formation.

Based on the above modification, Al Saedi et al. [4] presented an analytical model for the wellbore fluid temperature for a drilling circulation system in a vertical well, both in the drilling pipe (central tubing) and the annulus as a function of the well depth and the circulating time. Applying the appropriate initial and boundary conditions, the model predicts the fluid temperature both for the forward (injection by the central tubing) and the reverse (injection in the annulus) circulation mode and can be used also for coaxial vertical closed wells.

For the reverse circulation, which is of interest in the study, the fluid temperature in the annulus (denoted with the subscript *A*) and the central tubing (*T*) can be found by the below equations (after using the energy balances for the annulus and the tubing):

$$T_{f,A} = (1-\lambda_1 B)\alpha e^{\lambda_1 z} + (1-\lambda_2 B)\beta e^{\lambda_2 z} + g_T z + T_e(z=0) \tag{16}$$

$$T_{f,T} = \alpha e^{\lambda_1 z} + \beta e^{\lambda_2 z} + g_T z + T_e(z=0) + B g_T \tag{17}$$

where the coefficients λ_1 and λ_2 are given as:

$$\lambda_1 = \frac{-1+\sqrt{1+\dfrac{4C}{B}}}{2\Lambda} \tag{18}$$

$$\lambda_2 = \frac{-1 - \sqrt{1 + \frac{4C}{B}}}{2\Lambda} \tag{19}$$

The parameter C is similar with the Λ in Eq. (10) for Ramey's solution and B is the corresponding parameter for the tubing:

$$C = \frac{\dot{m}C_{pf}\left(k_e + r_{cf}U_A f_t\right)}{2\pi r_{cf}U_A k_e} \tag{20}$$

$$B = \frac{\dot{m}C_{pf}}{2\pi r_{ti}U_t} \tag{21}$$

U_A and U_T are the overall heat transfer coefficients of the annulus and the tubing, respectively, estimated by Eqs. (2) and (3).

The solution constants α and β can be found by applying the initial condition in the wellhead ($z = 0$) and the boundary condition at the bottom of the well ($z = L$):

$$T_{f,A}\big|_{z=0} = T_0 \tag{22}$$

$$T_{f,A}\big|_{z=L} = T_{f,T}\big|_{z=L} \tag{23}$$

Combining Eqs. (16)-(23) results in:

$$\alpha = \frac{[T_0 - T_e(z=0)]\lambda_2 e^{\lambda_2 L} + (1 - \lambda_2 B)g_T}{(1 - \lambda_1 B)\lambda_2 e^{\lambda_2 L} - (1 - \lambda_2 B)\lambda_1 e^{\lambda_1 L}} \tag{24}$$

$$\beta = \frac{-[T_0 - T_e(z=0)]\lambda_1 e^{\lambda_1 L} - (1 - \lambda_1 B)g_T}{(1 - \lambda_1 B)\lambda_2 e^{\lambda_2 L} - (1 - \lambda_2 B)\lambda_1 e^{\lambda_1 L}} \tag{25}$$

Recently, Sharma et al. [5] expanded further the above analysis and provided analytical solutions for a coaxial L-shaped closed well also considering the horizontal part. The equations for the vertical (denoted as V) and the horizontal (H) parts of the annulus and the tubing are:

$$T_{f,AV} = (1 - \lambda_1 B)\alpha_1 e^{\lambda_1 z} + (1 - \lambda_2 B)\beta_1 e^{\lambda_2 z} + g_T z + T_e(z=0) \tag{26}$$

$$T_{f,TV} = \alpha_1 e^{\lambda_1 z} + \beta_1 e^{\lambda_2 z} + g_T z + T_e(z=0) + B g_T \tag{27}$$

$$T_{f,AH} = (1 - \lambda_1 B)\alpha_2 e^{\lambda_1 z_H} + (1 - \lambda_2 B)\beta_2 e^{\lambda_2 z_H} + g_{TH} z_H + T_e(z=L) \tag{28}$$

$$T_{f,TH} = \alpha_2 e^{\lambda_1 z_H} + \beta_2 e^{\lambda_2 z_H} + g_{TH} z_H + T_e(z=L) + B g_{TH} \tag{29}$$

where z_H is the lateral distance in the horizontal part and g_{TH} is the geothermal gradient in the horizontal part. The coefficients λ_1 and λ_2 are the same as before and the solution constants α_1, α_2 and β_1, β_2 can be found by application of the initial condition in the wellhead ($z = 0$) and the boundary conditions at the heel ($z = L$) and at the bottom ($z = H$) of the well (H is the lateral length of the horizontal length):

$$T_{f,A}\big|_{z=0} = T_0 \tag{30}$$

$$T_{f,AV}\big|_{z=L} = T_{f,AH}\big|_{z_H=0} \tag{31}$$

$$T_{f,TV}\big|_{z=L} = T_{f,TH}\big|_{z_H=0} \tag{32}$$

$$T_{f,AH}\big|_{z_H=H} = T_{f,TH}\big|_{z_H=H} \quad (33)$$

A Python script was developed by IFPEN to solve the above system of equations. The solutions of Al Saedi and Sharma are used to benchmark the tools for the closed-loop test cases (vertical and horizontal, respectively) and are mentioned as Kabir's group solutions.

You's analytical solution

You et al. [6] provided a new derivation of Ramey's time function using Laplace transformation:

$$f_t = \mathrm{L}^{-1}\left[\frac{1}{\sqrt{s}}\frac{K_1(\sqrt{s})}{2\pi k_e R_\theta \sqrt{s} K_1(\sqrt{s}) + K_0(\sqrt{s})}\right] \quad (34)$$

where s is the Laplace variable, L^{-1} is the inverse Laplace transformation, K_0 and K_1 are the modified Bessel zero- and first-order, and R_θ is the wellbore's thermal resistance as in Eq. (3). In addition, the authors provided the Laplace transform of the heat conduction equation, the Laplace inverse transform of which yields a temperature profile inside the formation with respect to the radius and the time. Using a Stehfest algorithm, it is possible to transform Eq. (34) back to the time domain:

$$\frac{T(r,t) - T_f}{T_{inf} - T_f} = \frac{1}{u}\left[1 - \frac{K_0\left(\frac{r}{r_{cf}}\sqrt{u}\right)}{2\pi k_e R_\theta \sqrt{u} K_1(\sqrt{u}) + K_0(\sqrt{u})}\right] \quad (35)$$

The analytical solution of You et al. [6] has been integrated in IFPEN's tool and can be used to access the temporal evolution of the fluid and rocks temperature. In this case, Eq. (35) is applied at every cell along the well with the fluid temperature depending on time and depth.

The Table 1 summarizes all available analytical solution with their domain of application and limitations.

Table 1. Summary of analytical solutions with their domain of application, advantages, and limitations.

Solution	Domain	Geometry	Advantages	Limitations
Ramey [2]	Fluid	Single pipe	• Easy to use. • Rapid results. • Time step independent.	• Uniform domain. • Long time steps.
Modified Ramey [this work]	Fluid	Single pipe	• Easy to use & fast. • Heterogeneous domains. • Time step independent.	• Long time steps.
Kabir [3]	Fluid	Single pipe	• Fast to use & fast. • Time step independent. • Short time steps.	• Uniform domain.
Al Saedi [4]	Fluids	Coaxial vertical well	• Easy to use & fast. • Time step independent. • Short time steps.	• Uniform domain. • Vertical well.
Sharma [5]	Fluids	Coaxial Horizontal closed well	• Easy to use & fast. • Time step independent. • Short time steps.	• Uniform domain.
You [6]	Rocks	Single pipe	• Time step independent.	• Long simulation times. • Complicate application. • Requires a radial mesh. • Uniform domain. • Long time steps.

3.3 Numerical tools

COMSOL (VITO)

COMSOL Multiphysics® is a general-purpose software developed to solve numerically an in explicit and implicit fashion different physical phenomena, such as electromagnetic, solid mechanics, fluid and heat flow mechanics in open system and porous medias [7].

To benchmark the defined cases, two modelling approaches were implemented for the heat flow inside the wellbore depending on the nature of the flow: unidirectional or bi-directional (coaxial tubing).

For unidirectional fluid flow, the modelling approach considers 1D transient heat flow inside the wellbore. The heat flow, expressed in terms of temperature *T*, is modelled with the transport Eq. (36), which considers the velocity field *u* as known. The heat exchange with the surrounding rock is established via a wall heat source term *Q*. Other types of external sources of heat are represented with a second heat source term Q_s. For example, this term can be used to account for the heat released by a pumping unit installed in a well.

$$\rho_f A C_{pf} \frac{\partial T}{\partial t} + \rho A u \nabla \mathrm{T} = \nabla A k_f \nabla \mathrm{T} + Q + Q_s \tag{36}$$

On the other hand, diffusive transient 3D heat flow is considered inside the rock. Eq. (37) shows the heat flow equation inside the rock in terms of temperature *T*. The coupling between Eqs. (36) and (37) is achieved via the wall heat source term *Q*.

$$\rho_e C_{pe} \frac{\partial T}{\partial t} = \nabla k_e \nabla \mathrm{T} + Q \tag{37}$$

In the above equation C_{pe}, ρ_e and k_e are the rock specific heat at constant pressure, the density, and the thermal conductivity, respectively.

For bidirectional flow, like the one presented in concentric bottom whole heat exchanger, the wellbore is discretized together with the rock system, such as the problem is solved fully coupled using porous media flow and heat transfer Eqs. (38) and (39), respectively. Flow is considered steady state while the heat transport is transient. Thus, the rock, casing and tubing are considered to have no permeability and porosity while the wellbore fluid domain have a large permeability and a porosity of one.

$$\begin{aligned} \nabla(\rho_f v) &= \dot{m} \\ v &= -\frac{k_{perm}}{\mu}(\nabla p - \rho g) \end{aligned} \tag{38}$$

$$\begin{aligned} (\rho C_P)_{eff} \frac{\partial T}{\partial t} + \rho_f C_{pf} v \nabla T + \nabla \mathrm{q} &= Q_h \\ q &= k_{cond_{eff}}(\nabla T) \end{aligned} \tag{39}$$

k_{perm} is the rock permeability, *q* is the conductive heat flux, Q_h is the heat source, and the subscript *eff* corresponds to weighted by porosity.

To account for the convective heat transfer coefficient *h*, that is dependent on the Reynold's number, an equivalent approximated thermal conductivity coefficient $k_{equivalent}$ is computed for the casing and tubing following Eq. (40). Where k_{wall} is the equivalent casing or tubing conductivity, Δ_{wall} is the thickness of the casing and the tubing and *h* is the corresponding heat transfer coefficient.

$$k_{equivalent} = \frac{\Delta wall}{\left(\frac{1}{h} + \frac{\Delta wall}{k_{wall}}\right)} \quad (40)$$

Discretization of the rock domain can be done with either tetrahedral or radial elements. The latter are more suitable for vertical wells while tetrahedral elements can be used for complicated 3D domains like those related with horizontal wells.

GWellFM (IFPEN)

GWellFM (Geothermal Well Flow Model) is a steady-state, 1D non-isothermal axisymmetric, multicomponent, and two-phase flow simulator. The model considers the single-phase flows of liquids and gases, the hydrodynamics of the two-phase downward and upward flows, constitutive laws for mixtures and the heat exchange between the well completion and the surrounding formation [8].

For modelling the heat flow in the wellbore Eq. (6) is considered under steady-state conditions, whereas the heat transfer is modelled either under steady-state conditions applying the concept of thermal resistance in series until the infinity or under transient conditions solving numerically Eq. (1).

Apart from the numerical solution of the radial Fourier heat conduction equation, there is the option to perform simulations with Ramey's and You's analytical solution. In this case, at every axial cell the overall heat transfer coefficient of Eq. (2) is modified and calculated using the appropriate time function:

$$U = \frac{1}{2\pi r_{cf}\left(R_\theta + \frac{f_t}{2\pi k_e}\right)} \quad (41)$$

In addition, the model is fully compositional and, to perform thermodynamic calculations, a thermodynamic engine has been integrated into the code. Calculations are performed in thermodynamic equilibrium and several Equation-of-States are available (i.e., Cubic-Plus-Association, Peng-Robinson).

For the purposes of the study and to compare the results with the analytical solutions, the code was modified, and the same assumptions were applied. Thus, the transport properties of the fluids were kept constant, and the complete enthalpy balanced was replaced by the simplified, as described with Eq. (8) at steady-state conditions. It is worth mentioning that the simulator also solves the momentum balance along the well.

In the cases of a coaxial well (e and f), the simulator solves the momentum and the energy balances iteratively in a way that both pressure and temperature in the bottom cells of the central tubing and the annulus are matched. Starting with fixed injection pressure and temperature on the inlet side (annulus) and guessed outlet conditions (central tubing), the simulator modifies the outlet conditions until the below criteria are matched:

$$\frac{\left|P_{A,J} - P_{T,J}\right|}{P_{A,J}} < \varepsilon$$
$$\frac{\left|T_{A,J} - T_{T,J}\right|}{T_{A,J}} < \varepsilon \quad (42)$$

where ε is the convergence criterion (typical is 10^{-6}), and the subscripts *A*, *T*, *J* correspond to annulus side, tubing side and the last cell in the well.

Two types of meshes must be defined. An axial (vertical or horizontal) mesh along with flow in the wellbore, which consists of the fluid(s) and all solid materials (tubing, casing, cement, insulation) and a radial mesh in the formation. In the present study, the axial mesh was always regular with a constant

length, whereas the formation domain was always discretized with a geometric progression cells size. The mesh was refined close to the wall and size was gradually increased towards domain's border.

In all simulation cases, the time step was gradually increased by a factor until a maximum time step, according to the equation:

$$\Delta t_n = b\Delta t_{n-1},\ \Delta t_n \leq \Delta t_{max}$$
$$\Delta t_n = \Delta t_{max},\ \Delta t_n > \Delta t_{max} \quad (43)$$

where *n* is the number of the simulation and *b* is the increment factor.

GTW (IFE)

GTW (Geo-Thermal-Well) is a single-phase and semi-transient geothermal simulator in cylinder coordinates. The simulator solves the equation for transient heat conduction for cooling (or heating) of the rock, but it assumes stationary advective heat transport by the fluid in the well. The simulator obtains the numerical solution using an energy-conservative finite volume method. The energy transfer across cell boundaries is energy conservative in both the rock and the well. Local energy conservation for each cell implies global energy conservation for the combined system of well and rock. The temperature is given in the centre of the grid cells.

The temperature equation is solved for the rock and the well fully implicitly, using upstream differences for the heat advection in the inner tube and the annulus. This discretization scheme is unconditionally stable regarding the time-stepping. The time-stepping is controlled by the input parameters. The first time step for a normal simulation that spans several years is usually small, maybe just one minute. Then, the time step increases with a user-given factor until the maximum time step is reached. It is necessary to start with a small time step to pick up the early and strong temperature transient for cooling of the rock. After a year or several years of energy production, the temperature is changing slowly, and longer time steps can be used. The maximum time step can be several months. The number of time steps used is typically between 100 and 200.

The grid is in cylinder coordinates. The radial thickness of the inner tube, the insulation, the annulus and the three layers outside the well are user inputs to the simulator. The grid outside the outermost layer has a radial thickness that increases with a constant factor away from the well. The exception is the outermost cells. These cells have a hard-coded radial thickness of 1% of the radial extent of the model. The user input divides the grid into segments along the well, where each segment has a unique radius, and material properties, including rock properties and temperature gradient.

The simulator exports all parameters of each well segment and the operating conditions to a Python script. The segments are represented as a linked list of a class that is well-segment. The Python script serves as an interface to other analytical or numerical solutions for the equations of borehole heat exchangers.

With an almost incompressible fluid like water, the heat transport by the fluid depends mostly on the heat capacity. Then, the heat capacities at constant volume and at constant pressure are the same, and the heat transport does not depend on the pressure. In the general case of a compressible fluid, for example, supercritical CO_2, the enthalpy is linearized using the heat capacity at constant pressure and the thermal expansibility. The pressure and temperature are obtained in the well and the rock using an independent 1-D pipe simulator in an iterative manner. The pipe simulator provides a stationary pressure and temperature solution for the fluid in the well when the heat flux into the well is given by the geothermal simulator. The geothermal simulator then solves for the coupled temperature in the well and the rock using thermodynamic data from the 1-D pipe simulator. The heat flux into the well is then updated using the temperature field from the geothermal simulator. The temperature and pressure

converge after 2 or 3 iterations. Look-up tables provide all thermodynamic properties regarding pressure and temperature.

Summary of analytical and numerical tools

Table 2 summarizes the available analytical and numerical tools together with the advantages and disadvantages of each one. The description of the simulators used from each institute are summarized in the Annex A2.

Table 2. List of analytical and numerical tools with their capabilities and limitations.

User	Simulator	Model	Advantages	Disadvantages & limitations
All	Ramey	Analytical	• Easy • Fast • Solution independent of the previous time step.	• 1D • Constant fluid properties. • Only for long time scales. • No thermal interaction between fluids in coaxial wells. • Infinitely large domain.
IFPEN	Kabir		• Easy • Fast • Solution independent of the previous time step.	• 1D • Constant fluid properties. • No thermal interaction between fluids in coaxial wells. • Infinitely large domain.
	Sharma		• Easy • Fast • Solution independent of the previous time step. • Coaxial L-shaped closed well.	• 1D • No thermal interaction between fluids in coaxial wells. • Infinitely large domain.
	You		• Solution independent of the previous time step.	• 1D • Constant fluid properties. • Infinitely large domain. • Difficult to use. • Large simulation times.
VITO	COMSOL	Numerical	• 3D, thus irregular geometries like well with branches can be addressed. • Multiple physics like fluid flow in porous media for open-loop single well systems can be coupled.	• Setting the case for the first time can be a long process. Geometry and meshing construction are time consuming tasks. • It is not an open-source code. • Modelling explicitly the velocity field can be difficult due to the length scale of the problem and the level of discretization needed.
IFPEN	GWellFM	Numerical & analytical	• Easy to set-up both for opened and closed wells, with a tube or a coaxial well. • Solves the fluid flow and the heat transfer. • EoS to calculate transport properties. • Provides evolution of fluids temperature, pressure, properties, and rocks temperature • 2D heat transfer in the formation	• Time step depends on the geometry and the flow rate. • Long simulation times when considering the complete problem: very long wells, with not constant physical. • Axisymmetric. • It is not an open-source code.
IFE	GTW	Numerical	• Fast. • Easy to use. • 2D heat transfer in the formation in cylinder coordinates. • Tables for CO_2 and H_2O properties.	• Axisymmetric. • It is not an open-source code. • Always pipe-in-pipe configuration.

3.4 Case studies

To benchmark the different simulation tools intended to model closed-loop geothermal wells in later steps of the project, a series of cases were defined. The activity began with simple cases that have analytical solutions or analytical approximations for the fluid's temperature to compare with (Ramey's solutions). These cases were named: a, b, c, d (shown in Figure 3 and Figure 4). Then, more complex cases involving coaxial pipes in vertical and horizontal wells as well as multiple cement and casing layers were tested (shown in Figure 5 and Figure 6). For these cases, which were called e, f, g, h, the comparison was performed against Kabir's analytical solutions (cases e and f) and Ramey's analytical solution (cases g and h).

This comparison was performed in terms of temperature profiles along the well (annulus and inner tubing), considering different times. In all cases the total simulated time was fixed to 10 years.

Simple cases

The simple cases were elaborated following the conditions defined in the analytical solution of Ramey [2]. This analytical model aims to forecast the heat exchange in wellbores for incompressible unidirectional flow, i.e., coaxial tubing is not considered. When compared with geothermal closed-loop wells where injection is through the annulus, these cases correspond to having a returning inner tubing with small diameter and zero thermal conductivity. Figure 3 and Figure 4 illustrate the cases a, b, c, d, while Table 3,

Table 4, Table 5 and Table 6 show the corresponding input parameters. The description of the cases is given below:

- Case a: Vertical injector well. It consists of the injection of cold water in a fully cased vertical well that crosses a homogenous rock domain, which means the thermal conductivity, density and thermal heat capacity are constant with depth as shown in Figure 3. The analytical solution for this case was published by Ramey [2].

- Case b: Horizontal injector well. It addresses the injection of cold water in a cased horizontal well drilled in a homogeneous rock unit as shown in Figure 3. The analytical solution of Ramey was applied in series after straightening the horizontal part of the well (modified Ramey's solution). This approximation was used as a reference for benchmarking.

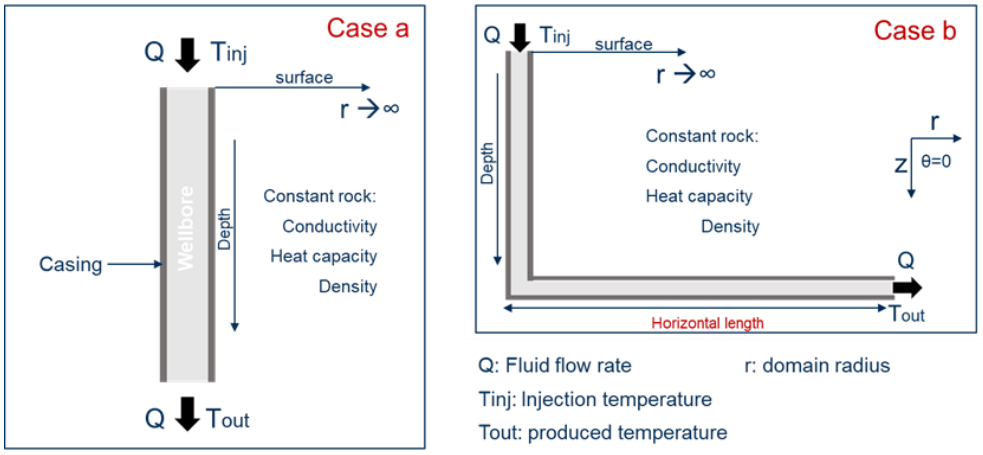

Figure 3. Illustration of case a (vertical well) and case b (horizontal well) used to benchmark the temperature forecasted by the different simulators.

- Case c: Vertical injector well crossing two layers. It tests the ability of the tools to handle vertical heterogenous rocks while injecting a hot fluid in a cased vertical well, as shown in Figure 4. This

case is based on the work of Wu & Pruess [9] and was compared against the analytical solution of Ramey.

- Case d: Horizontal injector well crossing two layers in its vertical section. It explores the tools capacity to handle horizontal wells drilled across vertical heterogeneous rocks, as shown in Figure 4. It was compared against the modified solution of Ramey applied in series.

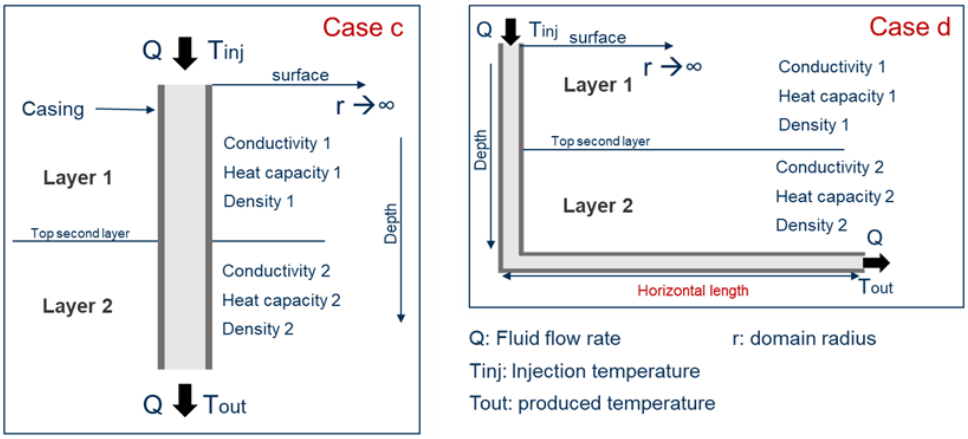

Figure 4. Illustration of case c (vertical well) and case d (horizontal well) used to benchmark the wellbore temperature forecasted by the different simulators.

Table 3. Well geometry description for simple cases used during the benchmarking.

Case	a	b	c	d
Completion	Totally cased	Totally cased	Open hole	Totally cased
Type of directional well	Vertical	Horizontal	Vertical	Horizontal
Vertical depth [m]	--	3000	--	3000
Horizontal section length [m]	--	3500	--	3500
Total depth [m]	1828.8	6500	1000	6500
Casing internal diameter [m]	0.1617	0.1617	0.1439	0.1617
Casing external diameter [m]	0.1778	0.1778	0.16	0.1778
Casing thermal conductivity [W/m/K]	43.268	43.268	43.268	43.268

Table 4. Underground description for simple cases used during the benchmarking.

Case	a	b	c	d
Rock thermal conductivity [W/m/K]	2.423	2.423	Layer 1: 2.8 Layer 2: 1.4	Layer 1: 2.423 Layer 2: 5.3
Bulk rock density [kg/m^3]	2600	2600	Layer 1: 2200 Layer 2: 1500	Layer 1: 2600 Layer 2: 3000
Rock specific heat capacity [J/kg/K]	902.67	902.67	Layer 1: 740 Layer 2: 800	Layer 1: 902.67 Layer 2: 534.9
Surface temperature [°C]	21.111	11	20	20
Thermal gradient [°C/m]	0.01513	0.0325	0.03	0.03
Layer 2 Top [m]	--	--	500	2900

Table 5. Wellbore fluid description for simple cases used during the benchmarking.

Case	a, b, c, d

Type of fluid	Water
Compressibility [bar^{-1}]	0
Heat capacity [J/kg/K]	4196
Density [kg/m^3]	998.554
Thermal conductivity [W/m/K]	0.5867
Viscosity [Pa.s]	0.0011

Table 6. Dynamic conditions for simple cases used during the benchmarking.

Case	a	b	c	d
Injection temperature [°C]	14.72	45.00	100.00	45.00
Fluid flow rate [kg/s]	8.8	8.8	1.1	8.8

Complex cases

These set of cases represent real geothermal closed-loop problems or more complex well completion and they were based on cases a and b by introducing a central tubing. The description of the cases is listed below while the corresponding illustrations and qualitative characteristics are shown in Figure 5 and Figure 6 , Table 7, Table 8, Table 9 and Table 10.

- Case e: Vertical coaxial closed-loop well. It represents a closed-loop system in a vertical well as shown in Figure 5, where an inner tubing is installed inside the wellbore until the bottom of the well. In this case, water is injected through the annular space formed by the casing and the inner tubing and circulated to the surface through the inner tube. Thus, the water is heated up as it flows down. Here, the effect of heat leakage from the inner tubing to the annulus is modelled. The results of the tools were compared with Kabir's solution (Al Saedi et al. [4]).

- Case f: Horizontal coaxial closed-loop well. It corresponds to a closed-loop system in a horizontal well as proposed in the HOCLOOP configuration. Thus, the inner pipe extends from the surface until the end of the horizontal well section (toe) as illustrated in Figure 5. Here, the effect of heat leakage from the inner tubing to the annulus is captured and the comparison is made with Kabir's solution (Sharma et al. [5]).

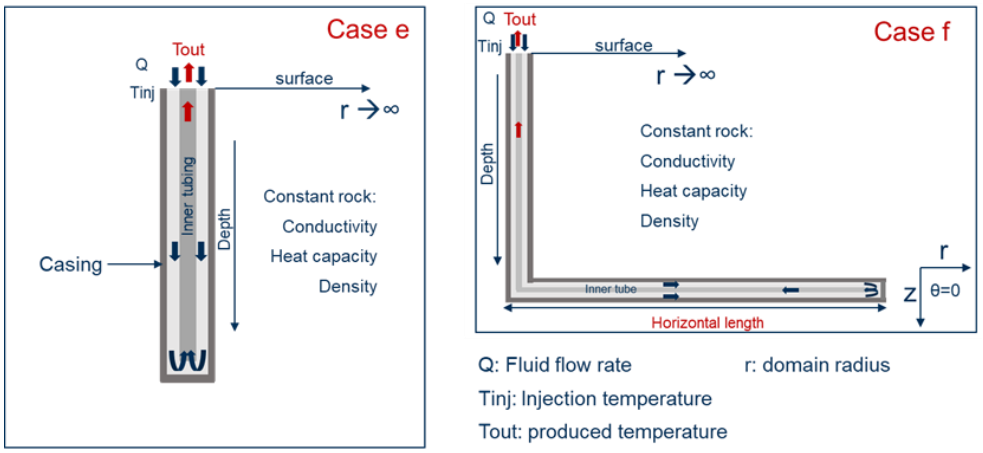

Figure 5. Illustration of case e (vertical well) and case f (horizontal well) used to benchmark the wellbore temperature forecasted by the different simulation tools.

- Case g: Cased and cemented vertical injector well. It evaluates how the tools handle the presence of a cement layer between the casing and the rock as can be seen in Figure 6.

- Case h: Multiple cement and casing layers in a vertical injector well. In this case it is tested the existence of different casing and cements layers with different depths as shown in Figure 6.

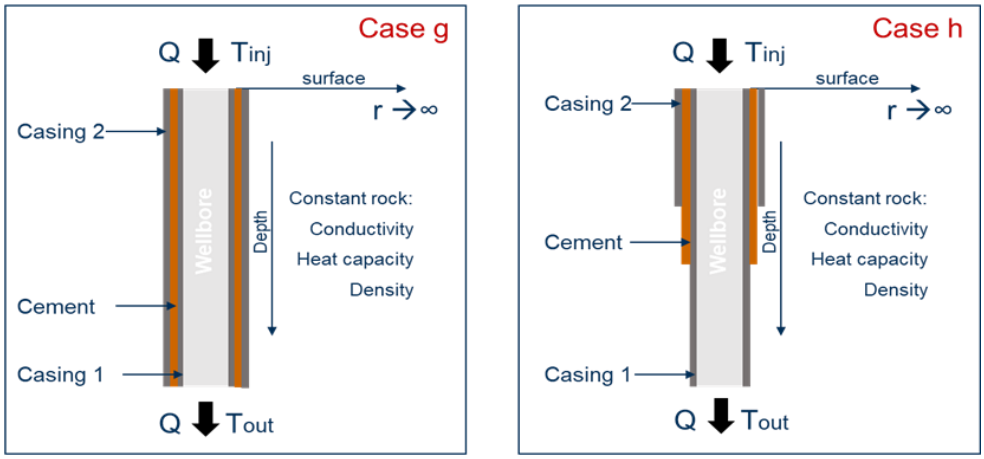

Figure 6. Illustration of case g (vertical well) and case h (vertical well) used to benchmark the wellbore temperature forecasted by the different simulation tools.

Table 7. Underground description for complex cases used during the benchmarking.

Case	e	f	g	h
Rock thermal conductivity [W/m/K]	2.423	2.423	2.423	2.423
Bulk rock density [kg/m^3]	2600	2600	2600	2600
Rock specific heat capacity [J/kg/K]	902.67	902.67	902.67	902.67
Surface temperature [°C]	21.111	11	21.111	21.111
Thermal gradient [°C/m]	0.01513	0.0325	0.01513	0.01513

Table 8. Well geometry description for complex cases used during the benchmarking.

Case	e	f	g	h
Type of well	Totally cased	Totally cased	Open hole	Totally cased
Orientation	Vertical	Horizontal	Vertical	Horizontal
Vertical depth [m]	--	3000	--	--
Horizontal section length [m]	--	3500	--	--
Total depth [m]	1828.8	6500	1828.8	1828.8
Casing internal diameter [m]	0.1617	0.1617	0.1617	0.1617
Casing external diameter [m]	0.1778	0.1778	0.1778	0.1778
Casing thermal conductivity [W/m/K]	43.268	43.268	43.268	43.268
Cement thermal conductivity [W/m-K]	--	--	2.476	2.476
Inner tubing internal diameter [m]	0.05	0.05	--	--
Inner tubing external diameter [m]	0.08	0.08	--	--
Inner tubing thermal conductivity [W/m/K]	0.1	0.1	--	--
Depth Cement [m]	--	--	1828.8	1000
Depth Casing 1 [m]	1828.8	1828.8	1828.8	1828.8
Depth Casing 2 [m]	--	--	1828.8	500
Cement thickness [m]	--	--	0.04	0.04

Casing 2 thickness [m]	--	--	0.007	0.007

Table 9. Wellbore fluid description for complex cases used during the benchmarking.

Case	e, f, g, h
Type of fluid	Water
Compressibility [bar^{-1}]	0
Heat capacity [J/kg/K]	4196
Density [kg/m^3]	998.554
Thermal conductivity [W/m/K]	0.5867
Viscosity [Pa.s]	0.0011

Table 10. Dynamic conditions for complex cases used during the benchmarking.

Case	e	f	g	h
Injection temperature [°C]	14.72	45.00	14.72	14.72
Fluid flow rate [kg/s]	8.8	8.8	8.8	8.8

Sensitivity to central tubing thermal conductivity

The case e was chosen to perform a sensitivity study and to evaluate the impact on the production of the central tubing thermal conductivity. This interface between the injection and the production fluid in coaxial closed wells serves as insulator, protecting the production fluid from losing heat towards the injection fluid. The values tested are given in the below table.

Table 11. Sensitivity to central tubing thermal conductivity of case e.

Case	e	e1	e2
Inner tubing thermal conductivity [W/m/K]	0.1	0.02	0.5

Sensitivity to mass flow rate

Similarly, the case e was chosen to perform a sensitivity study of the injection flow rate. Simulations with three different flow rates were performed, as per Table 12.

Table 12. Sensitivity to mass flow rate of case e.

Case	e3	e4	e5
Fluid flow rate [kg/s]	0.5	2	8

A summary of the tested scenarios is shown in Table 13.

Error and difference estimation

For comparison reasons the error, δ, is introduced to compare the temperature calculated with a reference method, i.e., Ramey's solution, and the temperature predicted by the simulators, T_{pred}:

$$\delta = \frac{T_{ref} - T_{pred}}{T_{ref}} 100 \quad (44)$$

The results of the different simulators are compared against Ramey solutions for specific times and at different depths in the well. For the coaxial wells, all simulators calculate the temperature along the

annulus part but also in the central tubing, whereas with Ramey solution only the temperature evolution in the annulus part is calculated.

Table 13. Summary of modelling scenarios.

Case	Type of well	Details
a	Vertical, injection	Constant rocks conductivity
b	Horizontal, injection	Combination of a vertical and a horizontal well
c	Vertical injection	Heterogenous formation (2 types of rocks)
d	Horizontal, injection	Heterogenous formation (2 types of rocks)
e	Vertical, coaxial, closed	Counter-current flow
f	Horizontal, coaxial, closed	Counter-current flow
g	Same as case e	Cased and cemented well
h	Same as case e	Partially cemented well
e1-2	Same as case e	Sensitivity to central tubing's thermal conductivity
e3-5	Same as case e	Sensitivity to mass flow rate

Difference between simulators, $\delta\,(\%)$, is also used to account for the variation of the results between the difference simulators.

$$\delta = \frac{T_{simulator[i]} - T_{simulator[j]}}{T_{simulator[i]}} 100, \qquad for\ i \neq j \tag{45}$$

Power estimation

For estimating the maximum theoretical production energy, *P* [W], the below equation is introduced for the coaxial cases e and e1-e5:

$$P = \dot{m}(H_{out} - H_{in}) = \dot{m}C_{pf}\left(T_{f,prod} - T_{f,inj}\right) \tag{46}$$

4. Results

4.1 Simple cases

The tree simulators, COMSOL (VITO), GTW (IFE) and GWellFM (IFPEN), were evaluated against analytical solutions. COMSOL and GTW model the heat flow in the rock by numerical approach while GWellFM has two options: numerical and analytical. The computed temperature profiles along the well for cases a, b, c and d and its graphical comparison with Ramey's analytical solution are shown next. In general, the results of the tested simulators follow the analytical results. Closer results were obtained with IFE's and IFPEN's simulators than with VITO's. The detailed results of all cases can be found at the annex section (A3-A6).

Case a

This case corresponds to the injection of water with a temperature lower than the rock temperature in a vertical well. All simulators predicted a continuous increase of the temperature as the water flows down in the well. These forecasts follow Ramey's analytical solutions as shown in Figure 7 and Figure 8 for different simulation times.

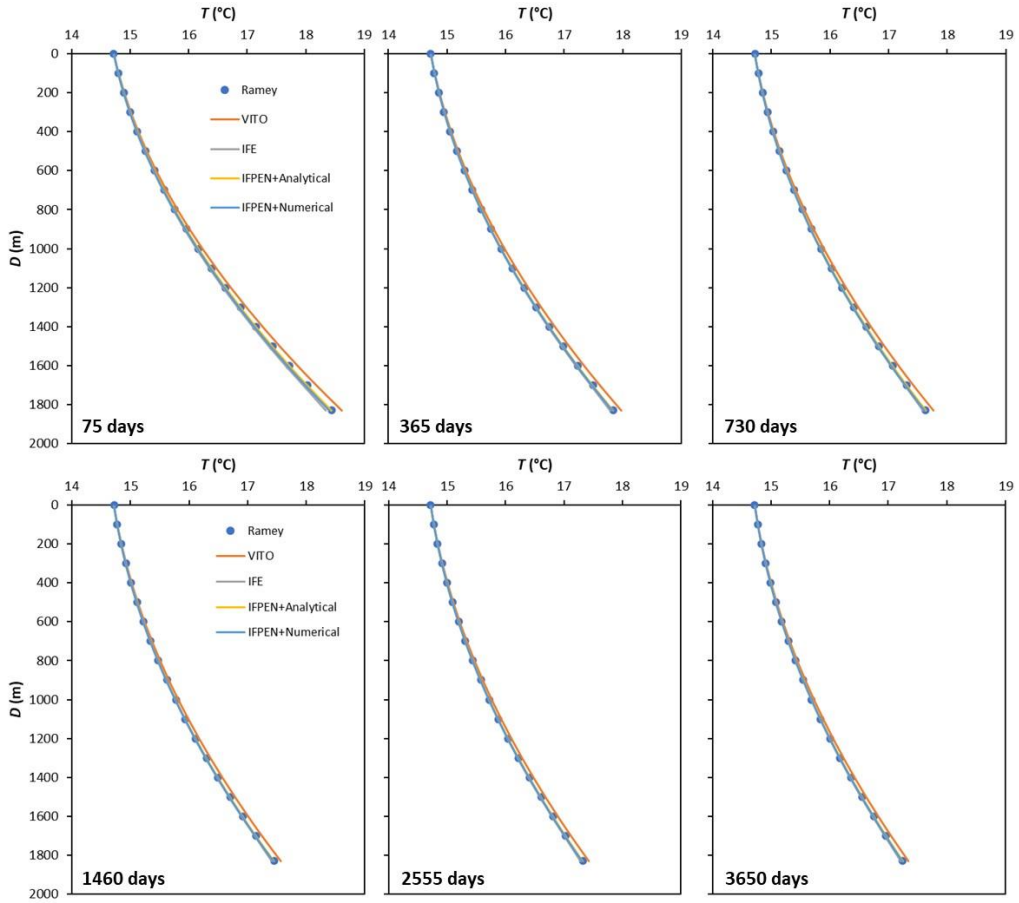

Figure 7. Comparison of fluid temperature along the well for case a at different times using the different simulators.

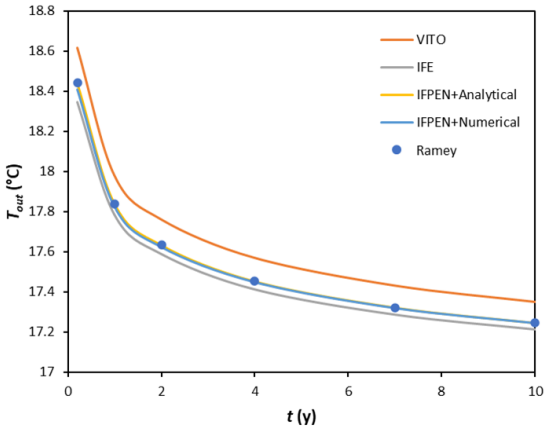

Figure 8. Comparison of the temporal evolution of the outlet temperature of the well of case a with Ramey's solution.

Case b

The heat exchange in a horizontal injector well without a returning pipe was evaluated in this case. IFE and IFPEN approximated the problem by converting the horizontal well in a pseudo-vertical well with 2 zones with different temperature gradients, representing the vertical and horizontal sections of the wells. While VITO model the problem in 3 dimensions. Results are shown in Figure 9 and Figure 10. The presence of the horizontal section with initial constant temperature makes the temperature profile to changes in slope. As previously, the simulations were able to follow the modified Ramey's solution, including the decrease in temperature at shallow depths due to heat leakage from the well to the surrounding rock. This is a situation that needs to be minimized in practical applications.

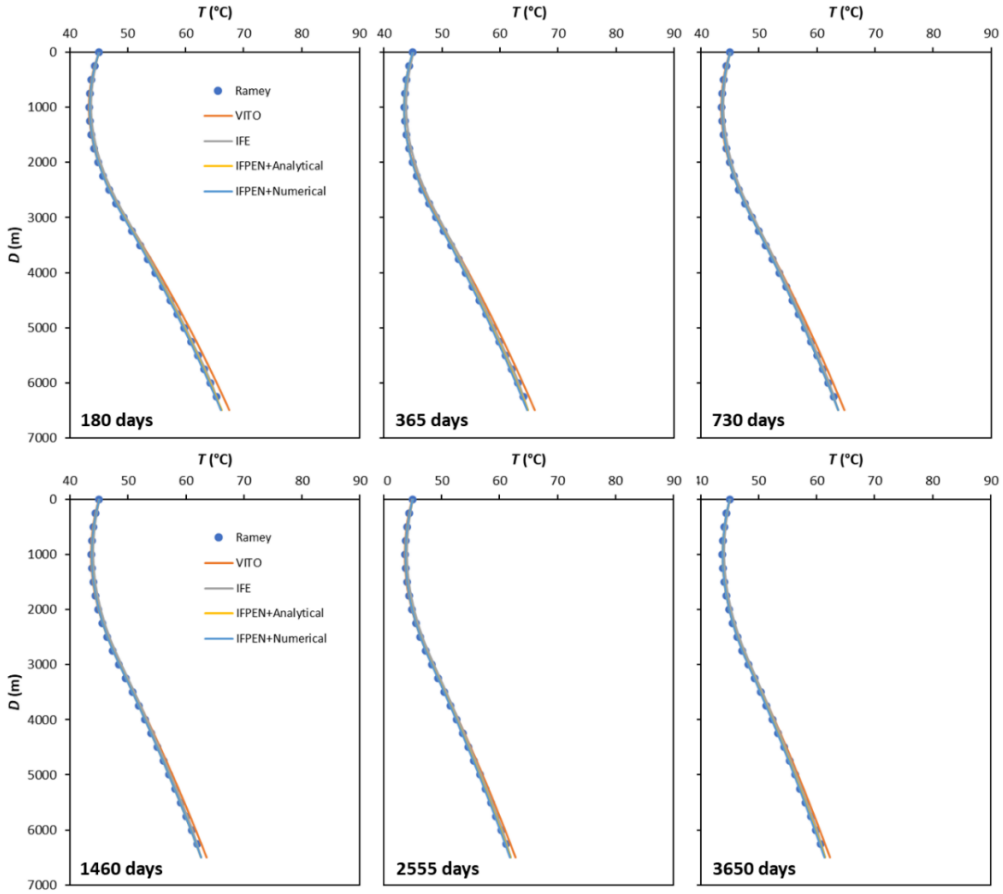

Figure 9. Comparison of fluid temperature along the well of case b at different times with Ramey's modified solution.

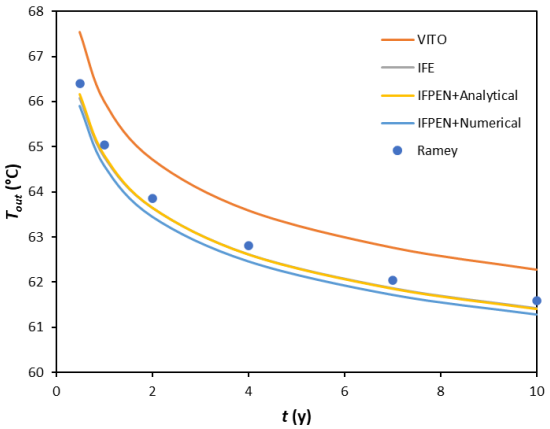

Figure 10. Comparison of the temporal evolution of the outlet temperature of the well of case b with Ramey's modified solution.

Case c

Cases c studied further the ability of the tools to model the heat leakage towards the formation in a vertical heterogeneous rock. Water was injected at 100°C, much higher than the maximum rock temperature, which was 50°C at 1000 m. Thus, heat leakage takes place along the well as shown in Figure 11 by the decreasing in fluid's temperature with depth. This heat leakage was modelled by all the tools in good agreement with modified Ramey's analytical solution. IFE's and IFPEN's simulators results are always overlapped in Figure 11 and Figure 12.

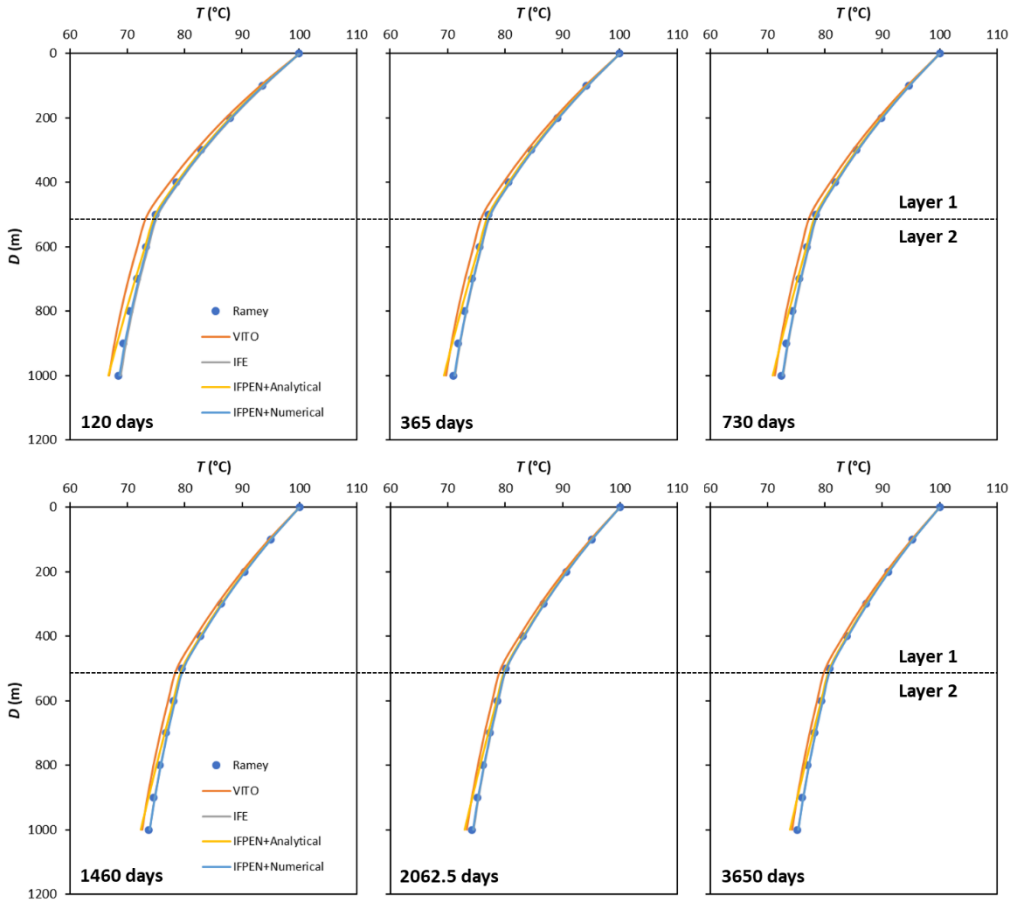

Figure 11. Comparison of the fluid temperature along the well of case c at different times.

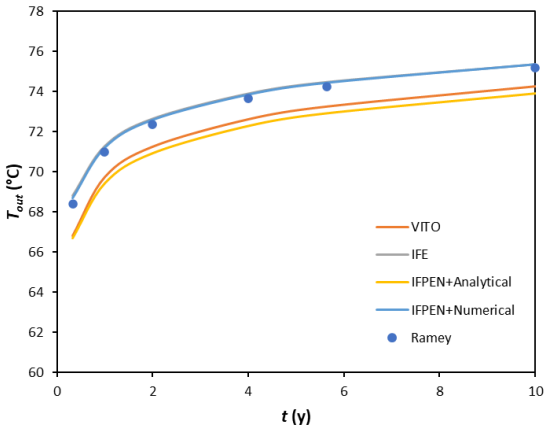

Figure 12. Comparison of the temporal evolution of the outlet temperature of the well of case c.

Case d

This case tested the effect of changing the rock thermal properties 50 m above the horizontal section of a well. The results and the corresponding comparison with the modified Ramey's solution are shown in Figure 13 and Figure 14. As in previous cases, all simulators provided the same temperature profile trend than the analytical solution. The closest results were obtained with IFE's and IFPEN's simulators (overlapping curves). Vito's results are affected by the maximum number of cells that can be handle in this large 3D domain.

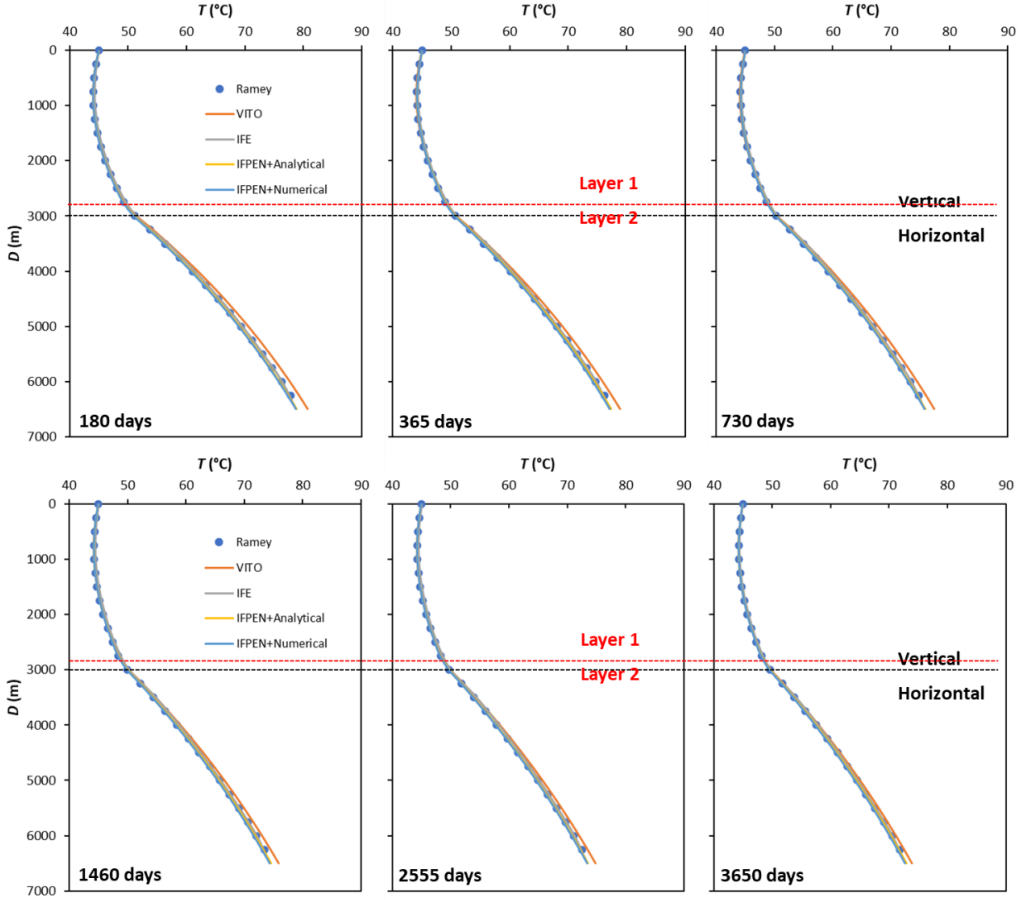

Figure 13. Comparison of the fluid temperature along the well of case d at different times.

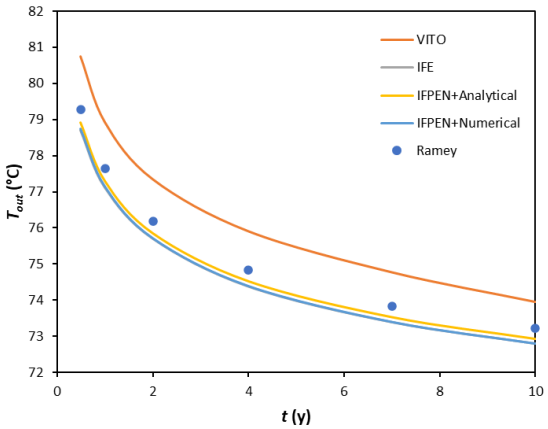

Figure 14. Comparison of the temporal evolution of the outlet temperature of the well of case d.

4.2 Complex cases

The complex cases can be separated into those that tested the coaxial flow presented in closed-loop applications (case f and cases e) and those concern to explore the capacity of the simulators to handle different well completion layers (cases g and h). The coaxial cases pose the more complex scenarios for modelling because they involved the heat transfer between counter-current fluid flows inside the well. Depending on the computational scheme, this may require explicit iterative process or fully couple strategies to solve the problem from the numerical point of view.

Case e

The heat extraction in a vertical well with a coaxial returning pipe was tested in this case. Therefore, the capacity of the simulators to model the heat losses in the returning tubing were evaluated against Kabir's analytical solution. Figure 16 depicts the temperature profile in the annulus (continuous line) and in the coaxial tubing (dashed line). In this case VITO and IFPEN's analytical simulators presents the closest results. IFPEN's numerical simulators presents a larger difference than IFPEN's analytical simulators as shown in Figure 15 and Figure 16, indicating that the main error is coming from the numerical approximation of the rock formation. This shows the error that numerical approximations can bring. It is important to mention that radial grids were used in the 3 simulators as well as that VITO's approach was to model the well-rock system fully coupled.

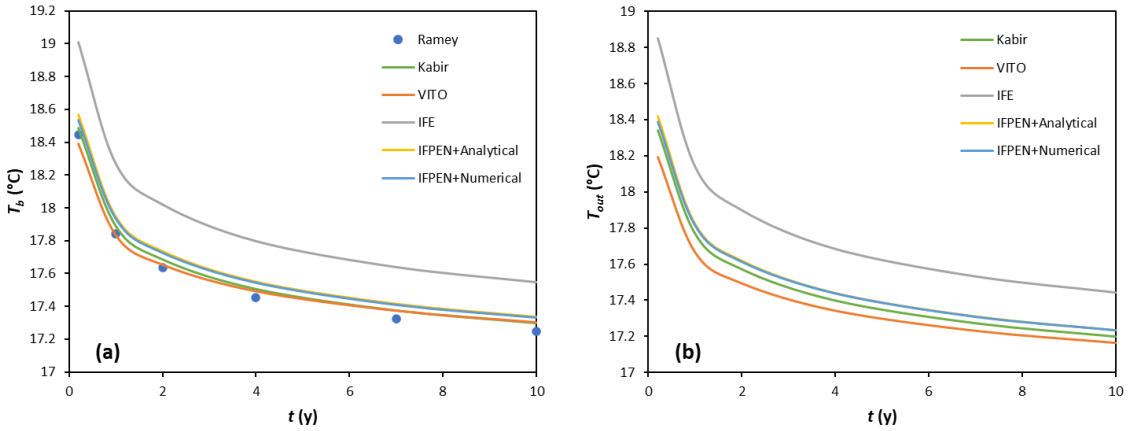

Figure 15. Comparison of the temporal evolution of (a) the temperature at the bottom of the annulus part and (b) the outlet temperature of the well against Kabir's analytical solution for case e.

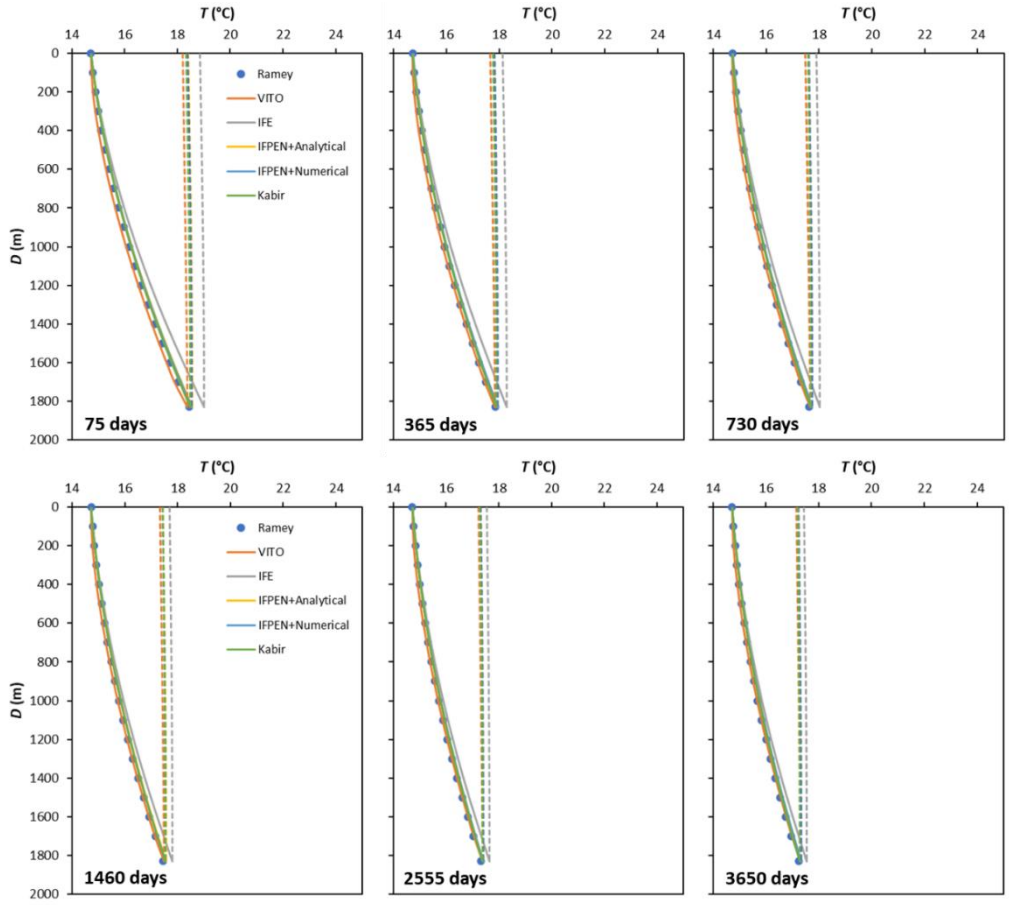

Figure 16. Comparison of the fluid temperature along the well of case e at different times (continuous lines: annulus side, dashed lines: tubing side)

Case f

In this case the ability of the simulators to model the coaxial closed-loop system in a horizontal well was evaluated. This case resembles the HOCLOOP concept. Radial grids were also used. Results are shown in Figure 17 and Figure 18. All simulators were able to model this case, but IFPEN's simulator obtained the closest solution to Kabir's analytical solution.

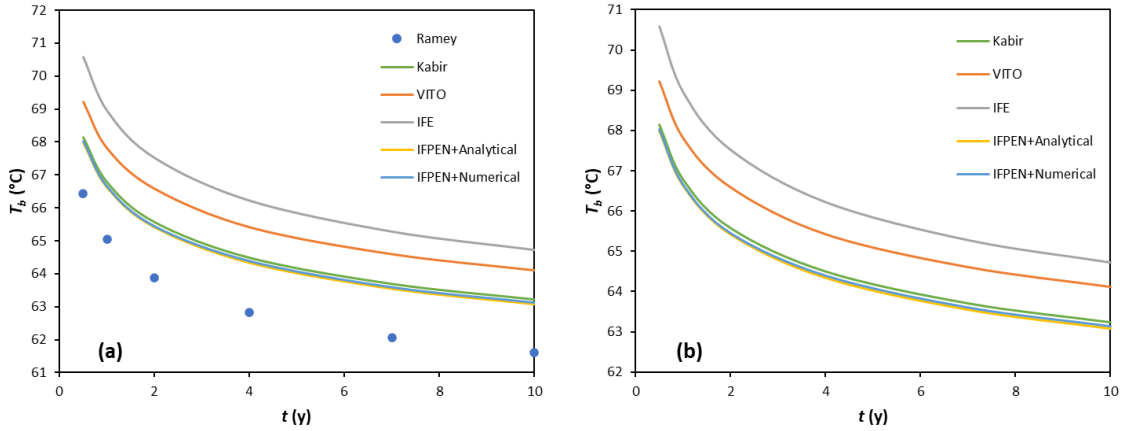

Figure 17. Comparison of the temporal evolution of (a) the temperature at the bottom of the annulus part and (b) the outlet temperature of the well against Kabir's analytical solution for case f.

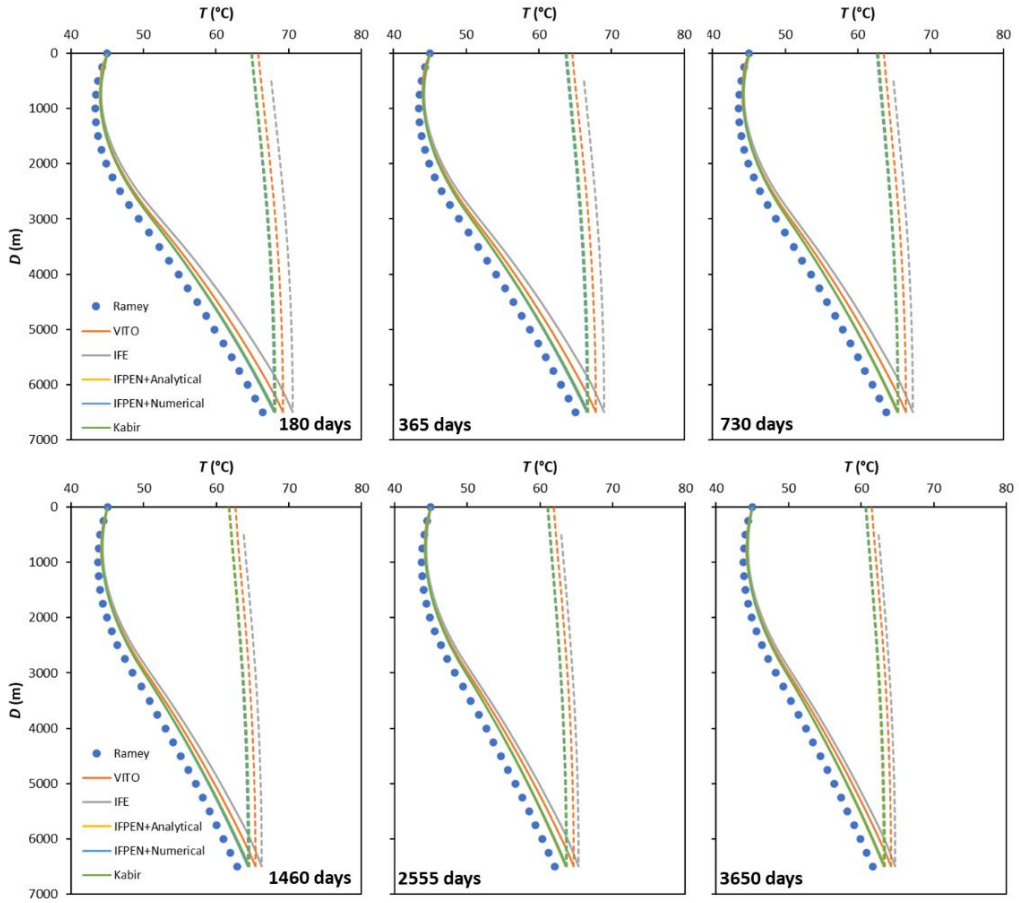

Figure 18. Comparison of the fluid temperature along the well of case f at different times against Kabir's solution (continuous lines: annulus side, dashed lines: tubing side)

Case g

Simulators were tested under a well completion comprising 2 casing and a cement layer that runs along a vertical well. This layer restricts the heat flow from the rock to the well and vice versa. The three simulators provided almost exact solutions when compared with Ramey's analytical solution as shown in Figure 19 and Figure 20.

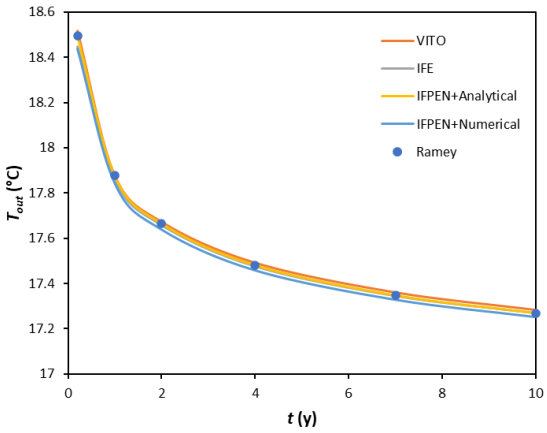

Figure 19. Comparison of the temporal evolution of the outlet temperature of the well of case g.

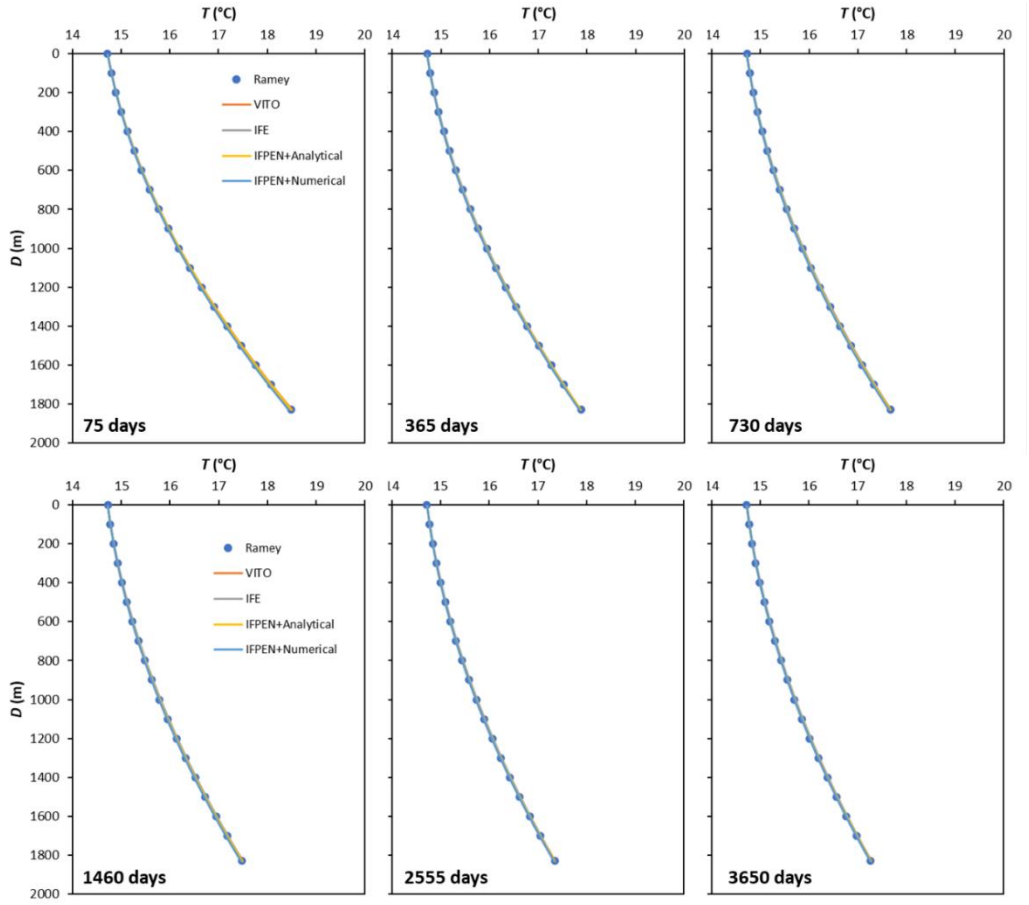

Figure 20. Comparison of the fluid temperature along the well of case g at different times.

Case h

This is a similar case as the previous one but with one of the casing and cement layers partially running along the well. For this case, IFE and IFPEN produced results almost the same as the analytical solution while VITO's solution is slightly more optimistic in terms of temperature during early times as shown in Figure 21 and Figure 22.

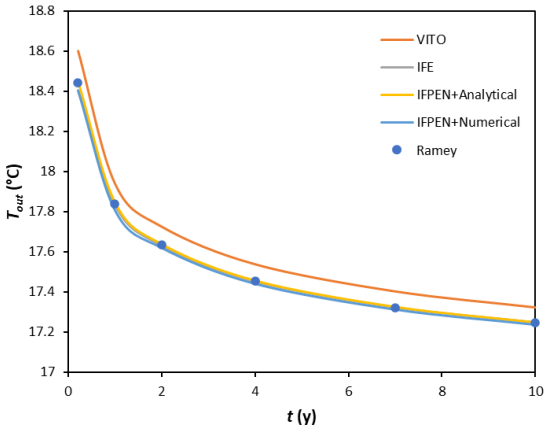

Figure 21. Comparison of the temporal evolution of the outlet temperature of the well of case h.

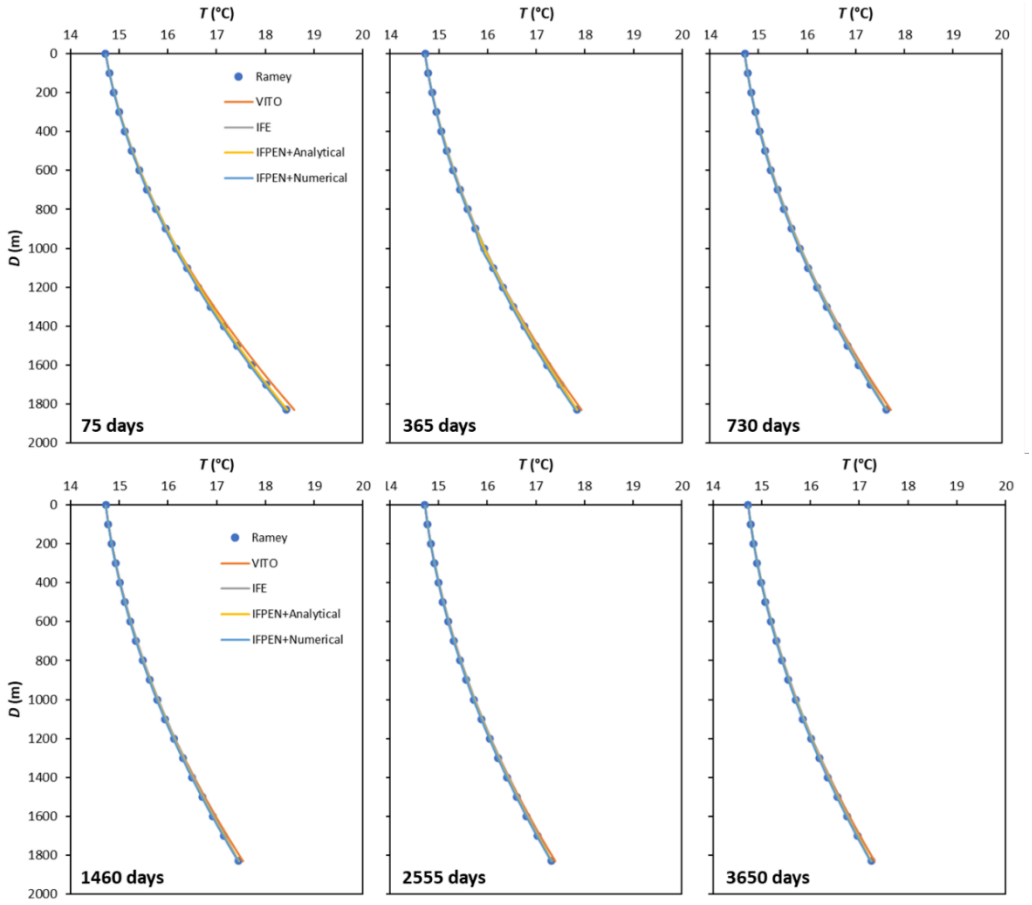

Figure 22. Comparison of the fluid temperature along the well of case h at different times.

4.3 Sensitivity studies

The effect of changing the fluid rate and the tubing conductivity on the simulator's temperature forecasts was analyzed. Coaxial systems in a vertical well, which corresponds to case 'e' was used as the based case for this sensitivity.

Mass flow rate

Three mass flow rates were evaluated: 0.5 kg/sec (case e3), 2 kg/sec (case e4) and 8 kg/sec (case e5). Temperature profiles in space and time can be found in the Annex A12. Figure 23 shows the estimation of the output temperature for two simulated times as a function of the circulation mass flow rate. As expected, the higher the flow rate the lower the output temperature. Additionally, it can be noticed that the differences between Kabir's analytical solution and the numerical simulators varies as a function of the mass flow rate, with the highest at the flow rate of 2 kg/sec. Nevertheless, when the analytical solution is used for modelling the heat flow in the rock (IFPEN-Analytical) the differences with the analytical solution are almost negligible and independent of the flow rate. The numerical approximation of the heat flow in the rock is responsible for the difference with the analytical solution.

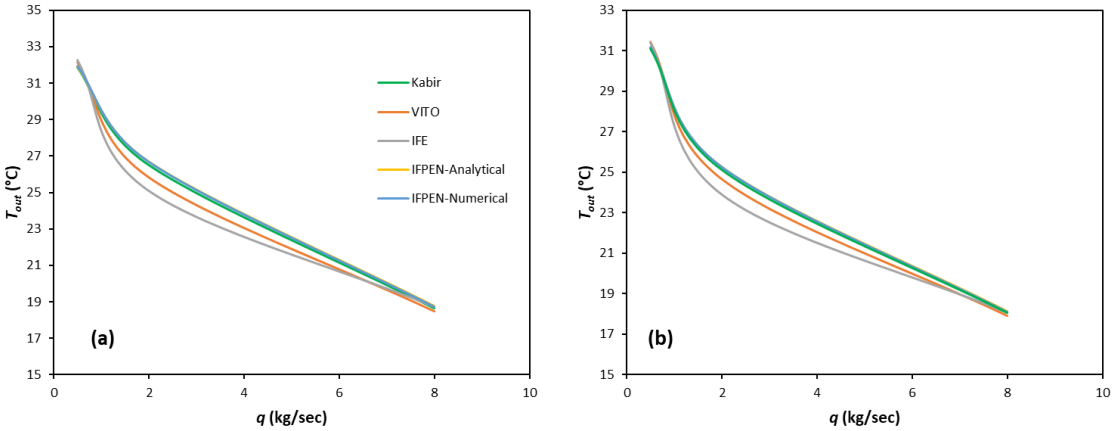

Figure 23. Effect of the mass flow rate on the outlet temperature differences between Kabir's analytical solution and the simulators after (a) 75 days and (b) 365 days.

Regarding the physical impact of changing flow rates on the output temperature, Figure 24 and Figure 25 show that the higher the flow rate the lower the produced temperature and the lower the temperature drop along the tubing. This is the result of a larger mass flow to be heated up and a higher flow velocity in the tubing when the mass fluid rate is increased. The corresponding power produced is shown in Figure 26. It is evident that the higher the flow rate is the higher the produced power is but the lower the output temperature is.

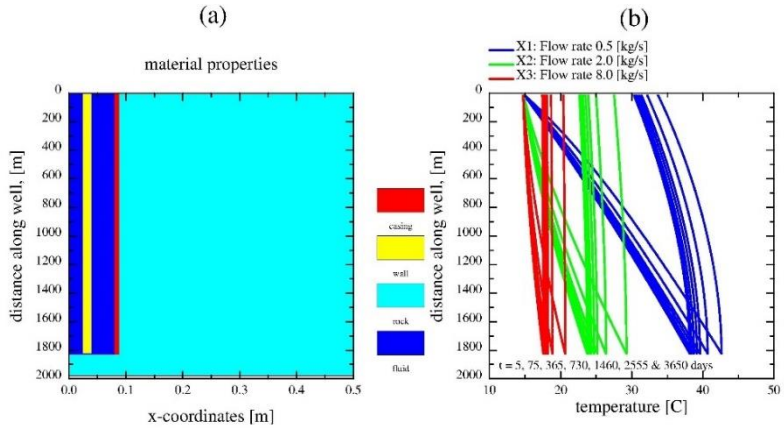

Figure 24. (a) Well configuration. (b) Fluids temperature at different times for the tested flow rates.

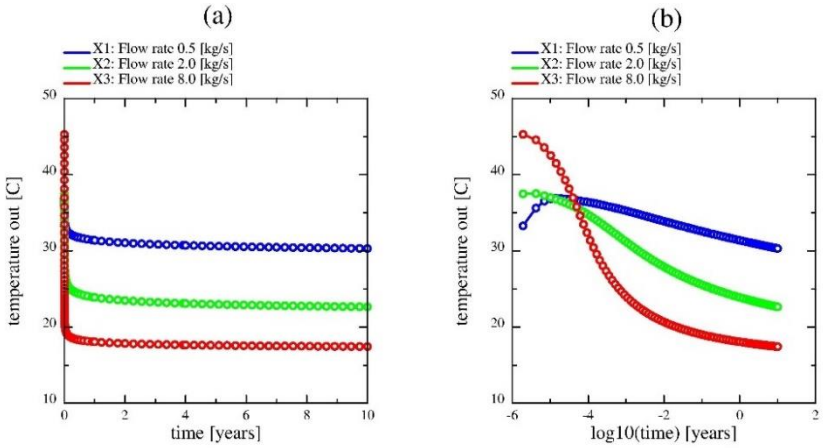

Figure 25. (a) The output temperature as a function of time for the three cases of tubing insulation. (b) The output temperature as a function of log10 of time.

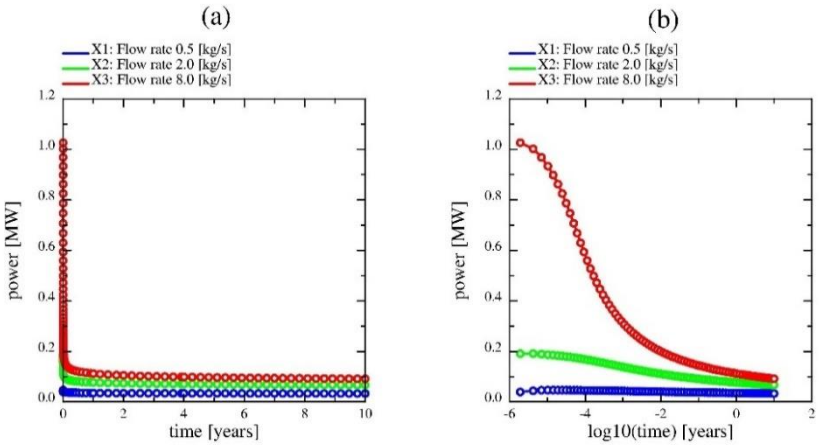

Figure 26. (a) The output power as a function of time for the three cases of flow rates. (b) The output power as a function of log10 of time

Tubing thermal conductivity

Similarly, the effect of tubing thermal conductivity was also tested in case e. Detailed results are found in Annex A11. For the evaluated conductivity range (0.02, 0.1 and 0.5 W/m/K) the differences between Kabir's analytical solution and the numerical simulators used by IFE and IFPEN show more variable behaviour than VITO and the analytical simulator used by IFPEN (IFPEN-Analytical), as shown in Figure 27.

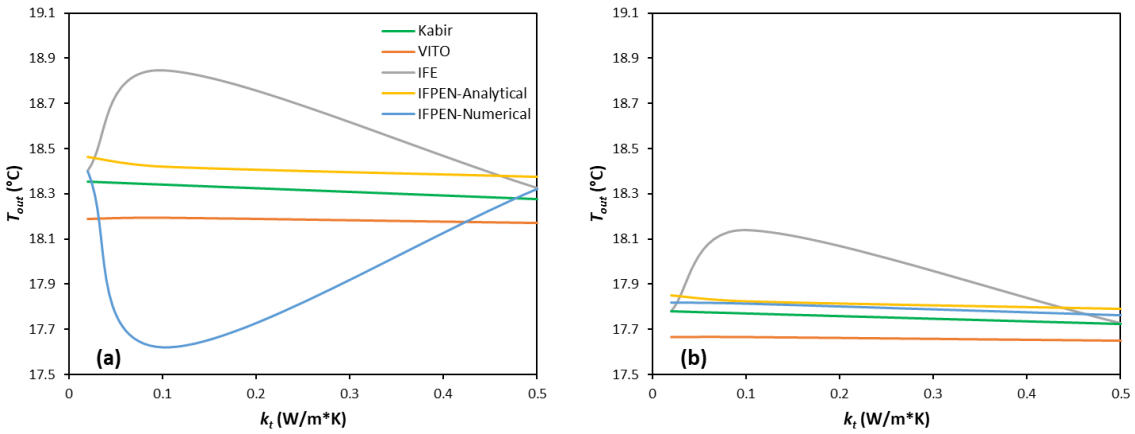

Figure 27. Effect of tubing conductivity on the outlet temperature and differences between Kabir's analytical solution and the simulators at (a) 75 days and (b) 365 days.

The effect of the different tubing thermal conductivities on the produced temperature and power are shown in Figure 28, Figure 29 and Figure 30. For the evaluated conductivity, no major changes in the produced temperature and power can be seen for late times. The major effects take place at early times. Regarding this case, there is no need to install a tubing with an ultralow thermal conductivity. For longer wells, the conclusion could be different.

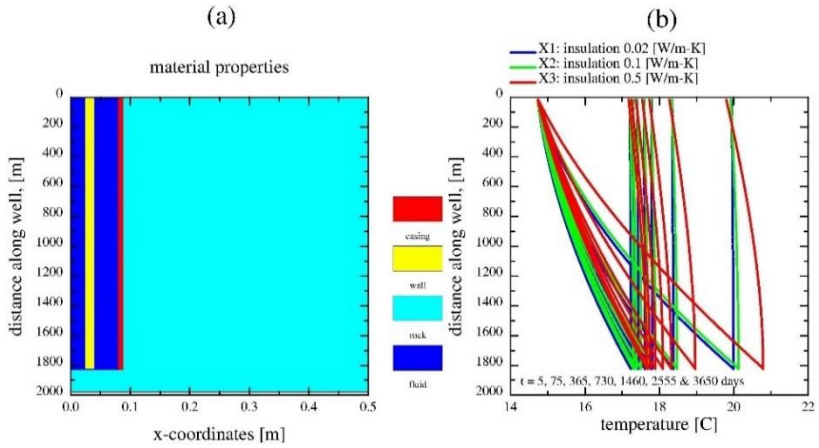

Figure 28. (a) Well configuration. (b) Well temperature at times 5, 75, 365, 730, 1460, 2555 and 3650 days.

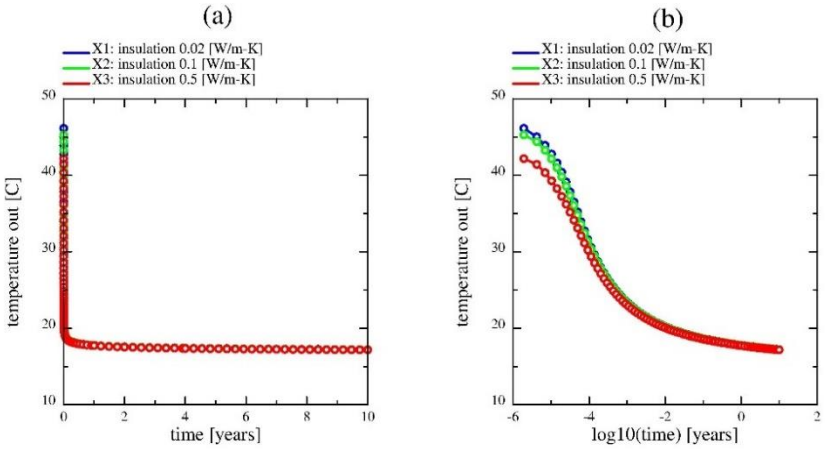

Figure 29. (a) The output temperature as a function of time for the three cases of tubing insulation. (b) The output temperature as a function of log10 of time.

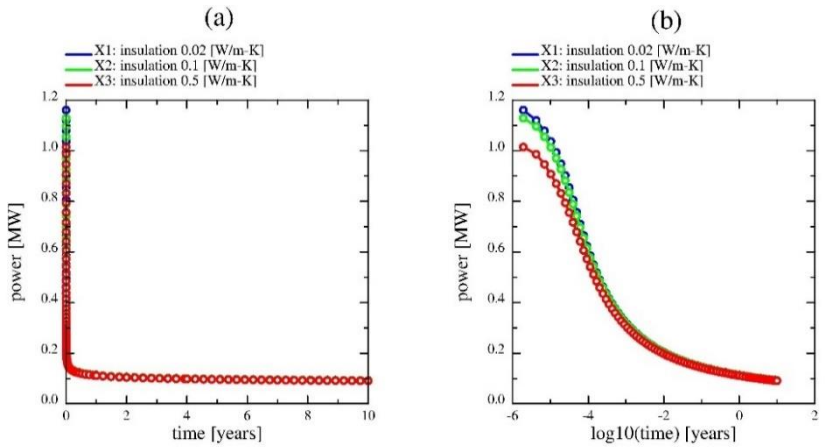

Figure 30. (a) The output temperature as a function of time for the three cases of tubing insulation. (b) The output temperature as a function of log10 of time.

5. Discussion

Three simulators were benchmarked for modelling heat exchange in wellbores: COMSOL (VITO), GWellFM (IFPEN) and GTW (IFE). All benchmark cases were completed by the three simulators as shown in the results chapter.

5.1 Accuracy

To quantify the accuracy of the simulators in modelling the heat transfer between the wellbore and the hosting formation, their results were compared against analytical solutions in terms of error expressed by Eq. (45). Figure 31 and Table 14 show the maximum and the average errors based on all computed points along the well. Ramey's analytical solution was used as a reference for cases a, b, c, d, g and h while Kabir's analytical solutions were used for cases e, f, e1 to e5. All tools show a good agreement when compared to the analytical solutions, with an average error below 5%.

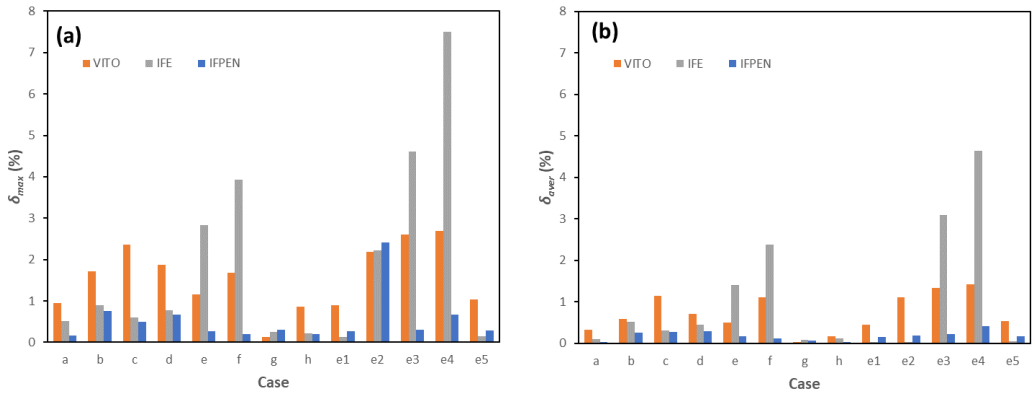

Figure 31. Summary of (a) the maximum and (b) the average error (%) in the wellbore temperature estimation when comparing all tools with Ramey's solution for cases a, b, c, d, g and h and with Kabir's for cases e, f, e1, e2, e3, e4 and e5.

Table 14. Summary of maximum and average error (%) when comparing the outlet temperature of the fluid of all tools with Ramey's or Kabir's solutions.

Case	COMSOL (VITO)		GWellFM (IFPEN)		GTW (IFE)	
	Average [%]	Maximum [%]	Average [%]	Maximum [%]	Average [%]	Maximum [%]
a	0.325	0.956	0.031	0.171	0.096	0.506
b	0.594	1.713	0.259	0.753	0.525	0.894
c	1.143	2.362	0.273	0.491	0.303	0.591
d	0.711	1.868	0.288	0.677	0.455	0.773
e	0.501	1.155	0.167	0.269	1.403	2.829
f	1.102	1.674	0.122	0.207	2.378	3.924
g	0.034	0.136	0.070	0.301	0.088	0.252
h	0.178	0.869	0.033	0.206	0.116	0.224
e1	0.454	0.902	0.153	0.261	0.040	0.128
e2	1.106	2.180	0.187	2.419	0.035	2.220
e3	1.342	2.612	0.228	0.300	3.088	4.610
e4	1.425	2.694	0.413	0.663	4.642	7.503
e5	0.537	1.038	0.169	0.289	0.043	0.140

The simple cases or the cases, where only one flow compartment exists in the well (without central tubing), presented an average error equal or lower to 1%. IFE's and IFPEN's simulators obtained closer

results than VITO's simulator for these cases. The difference is the type of grid used for discretizing the rock domain. IFE and IFPEN used radial cells while VITO used tetrahedral cells. Radials cells adapts better to the flow in the near wellbore region while tetrahedral can adapt easily to more irregular 3D domains like the one presented in deviated and horizontal wells.

The simulation results for coaxial closed-loop systems in vertical and horizontal wells (case 'e' and case 'f' respectively), however, show different behaviour. The average error is larger than the simple cases. This is the result of the numerical coupling scheme to simultaneously model the heat transfer between the rock and the annulus and between the annulus and the tubing.

Cases 'e' also shows that the error is a function of the flow conditions and material properties in all simulators. For example, GTW simulator obtained almost identical solutions than the analytical solution for cases e1, e2 and e5 but also presented the largest error in cases e3 and e4.

In most of the simulated cases, the maximum errors were observed at the end (bottom) of the well. All models start with the same injection temperature and as the calculations proceed towards the output, the impact of each solution method becomes more pronounced as shown in Figure 32.

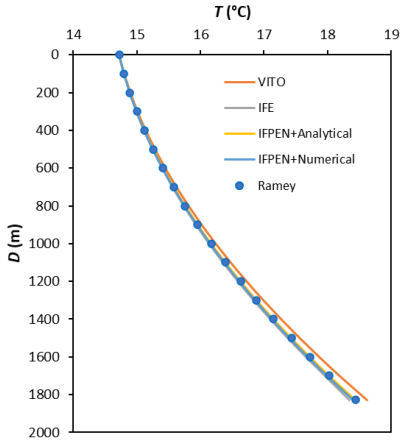

Figure 32. Comparison of the spatial evolution of the outlet temperature of the fluid after 75 days for case a.

The maximum and average differences when the simulators are compared among each other are shown in Figure 33 and Table 15. The simulators obtain similar results, the highest average difference is 5% for case 'f' between IFE and IFPEN. Another observation is that COMSOL and GWellFM provide closer results than when they are compared with GTW simulator.

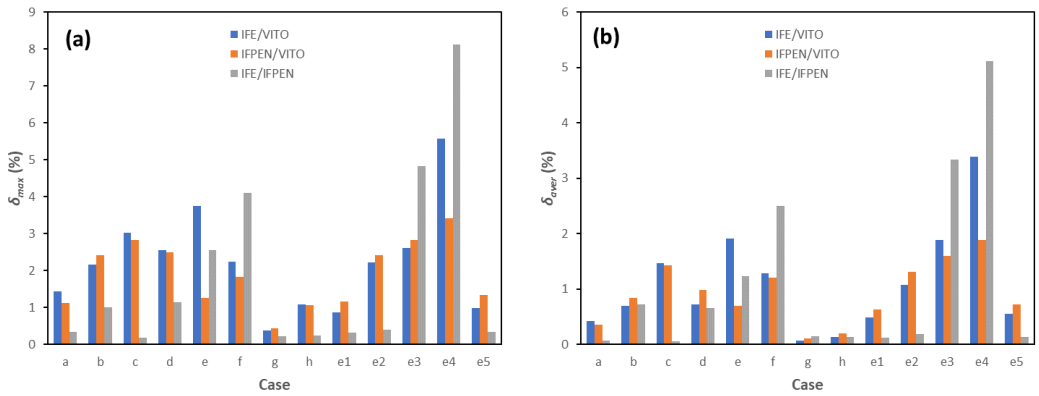

Figure 33. Summary of (a) the maximum and (b) the average error (%) when comparing the outlet temperature of the fluid between the tools for all benchmark cases.

Table 15. Summary of the maximum and the average error (%) when comparing the fluid temperature at the bottom hole of the annulus (A) and at the outlet of the tubing (T) of all tools with Kabir's solutions for the closed coaxial benchmark cases.

Case	COMSOL (VITO)				GWellFM (IFPEN)				GTW (IFE)			
	A		*T*		*A*		*T*		*A*		*T*	
	Aver.	**Max.**	**Aver.**	**Max.**	**Aver.**	**Max.**	**Aver.**	**Max.**	**Aver.**	**Max.**	**Aver.**	**Max.**
e	0.648	1.155	0.354	0.803	0.104	0.269	0.230	0.269	0.902	2.829	1.903	2.829
f	0.812	1.674	1.393	1.583	0.070	0.207	0.174	0.207	1.900	3.924	2.857	3.575
e1	0.463	0.785	0.445	0.902	0.089	0.236	0.217	0.261	0.046	0.128	0.034	0.054
e2	1.581	2.180	0.631	1.037	0.135	2.419	0.238	0.304	0.049	2.220	0.022	0.098
e3	1.866	2.612	0.818	1.395	0.208	0.300	0.249	0.296	3.895	4.610	2.282	3.564
e4	1.213	1.815	1.637	2.694	0.293	0.628	0.533	0.663	3.718	7.203	5.565	7.503
e5	0.603	0.954	0.471	1.038	0.101	0.263	0.237	0.289	0.052	0.140	0.035	0.058

5.2 Heat flow state

It is also worth mentioning that for all simulated cases the temperature is in transient conditions, which means that the temperature disturbance has not reached the outer boundary of the models during simulated times as shown in Figure 34. The low thermal conductivity of the rock is responsible for this behaviour. Nevertheless, in situations where more than one well is drilled in the same area, heat flow interference could take place if the well spacing is limited, this could result in the heat flow behaving in pseudo-steady state. In practice this means that larger temperature drops versus time will take place in this state than in transient state.

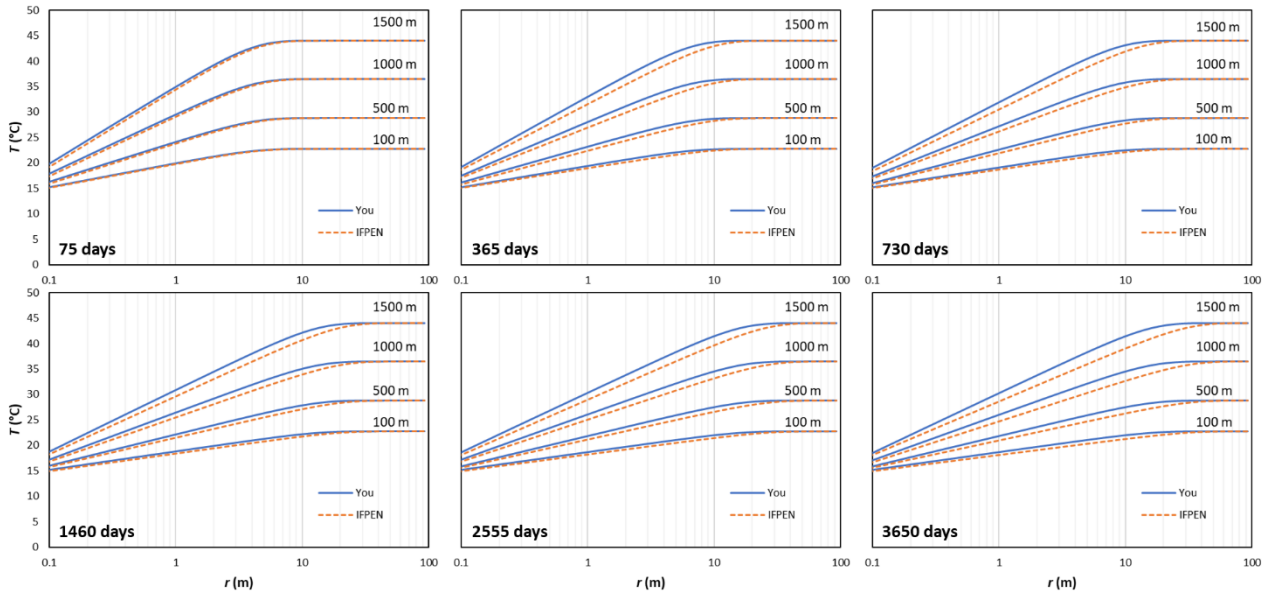

Figure 34. Comparison of temperature profiles in the rock domain at various depths and times between IFPEN's model and You's analytical model for case a.

5.3 Comparison of the three simulators

Table 16 compares the simulators in terms of accuracy, ease to set up a case and additional capabilities. A detailed comparison between the simulators can be found in Annex A3 to A10. For problems related with closed-loop single well systems GTW and GWellFM are better suited than COMSOL because they are easier to set up. For problems that involve complex trajectories or the coupling with other physics like fluid flow in porous and fracture media, COMSOL is an option to consider.

Table 16. Tested simulators comparison.

User	Simulator	**Setting up**	**Accuracy**	**Additional capabilities**
VITO	COMSOL	COMSOL is a general Finite Element Code. Thus, the initial setup of a case is not straight forward. The most time-consuming tasks are domain definition and gridding.	Accuracy depends on the type of grid: Tetrahedral or radial. For these problems, radial grid offers better results. Average error ranges between 1% to 2%	Interference between wells. It can be coupled with groundwater flow. The single well can be also modelled as an open system exchanging mass with ground water systems.
IFPEN	GWellFM Numerical	Easy	Good accuracy. Radial cells are used. Average error ranges between 0.03% to 0.4 %	
IFE	GTW	Easy	Average error ranges between 0.04% to 4.6 %	

6. Conclusions

Three different simulators were compared on the same well heat exchange benchmark cases: COMSOL (VITO), GWellFM (IFPEN) and GTW (IFE). All benchmark cases were completed by the three simulators and compared with the corresponding analytical solutions.

All the simulators can model conductive heat exchange in vertical and horizontal wells, including closed-loop well completions like the HOCLOOP concept. They can also account for vertical heterogeneous rocks, changing temperature gradients and wells with multiple walls (i.e., casing, cement, insulation) and complex geometries (i.e., changing diameter along the well).

For cases that involved injection of a fluid without recirculation (the injected fluid is not coming back to the surface), the simulators presented an average error lower than 1.1% when compared to Ramey's analytical solution. GWellFM and GTW having the best accuracy for the tested cases with average error less than 0.5%.

The average error of the simulators when modelling closed-loop cases (such as the HOCLOOP concept), was equal or lower than 4.6%. Thus, the present of a returning pipe and flow introduce more complexity and increases the error. For these cases, the flow conditions and well completion properties affect the accuracy of the simulator's solutions. For instance, the average error for GTW increases from 0.035% and 4.62% when flow rate was deceased and tubing thermal conductivity was increased. On the other hand, COMSOL showed more stability but also variable average errors that ranged from 0.5% and 1.42%. GWellFM's average errors were lower for all simulated cases (< 0.5%).

The simulators can capture the effect of different flow rates and pipe thermal properties. For instance, as the fluid injection rate is increased, the fluid losses in the returning pipe are minimized and the power production is maximized. Nevertheless, the produced temperature is reduced.

Irregular domains are a challenge for GWellFM and GTW simulators, as the domain discretization is done with radial grids. It is important to mention that radial grids are the best option for modelling near wellbore heat flow. The challenges could arise in problems with multiple wells or wells with multiple branches, where well interference can be important. On the other hand, COMSOL can handle these irregular domains by using unstructured grids.

Various analytical solutions to forecast the heat production from closed-loop geothermal systems in vertical and horizontal wells are available in the literature. These solutions address vertical and horizontal wells with homogeneous properties in the radial direction and incompressible recirculation fluids. In this work, an extension of Ramey's analytical solution for horizontal wells and/or heterogeneous formation was proposed and used during the benchmarking process. Nevertheless, these solutions can be introduced in in-house tools (as has been done in GWellFM) to account for more complex problems.

7. References

[1] M. Massoud, Engineering Thermofluids: Thermodynamics, Fluid Mechanics, and Heat Transfer, Berlin, Heidelberg: Springer-Verlag, 2005.

[2] H. Ramey Jr., "Wellbore heat transmission," *Journal of Petroleum Technology,* vol. 14, pp. 427-435, 1962.

[3] A. Hasan and C. Kabir, "Aspects of Wellbore Heat Transfer During Two-Phase Flow," *SPE Production & Facilities,* vol. 9, pp. 179-185, 1994.

[4] A. Al Saedi, R. Flori and C. Kabir, "New analytical solutions of wellbore fluid temperature profiles during drilling, circulating, and cementing operations," *Journal of Petroleum Science and Engineering,* vol. 170, pp. 206-217, 2018.

[5] P. Sharma, A. Al Saedi and C. Kabir, "Geothermal energy extraction with wellbore heat exchanger: Analytical model and parameter evaluation to optimize heat recovery," *Renewable Energy,* vol. 166, pp. 1-8, 2020.

[6] J. You, H. Rahnema and M. McMillan, "Numerical modeling of unsteady-state wellbore heat transmission," *Journal of Natural Gas Science and Engineering,* vol. 2016, pp. 1062-1076, 2016.

[7] "COMSOL Documentation," [Online]. Available: https://doc.comsol.com/6.0/docserver/#!/com.comsol.help.comsol/helpdesk/helpdesk.html. [Accessed March 2023].

[8] V. Leontidis, P. Niknam, I. Durgut, L. Talluri, G. Manfrida, D. Fiaschi, S. Akin and M. Gainville, "Tools for Modelling Reinjection of Two-Phase Non-Condensable Gases and Water in Geothermal Wells," *Applied Thermal Engineering,* vol. 223, p. 120018, 2023.

[9] Y.-S. Wu and K. Pruess, "An Analytical Solution for Wellbore Heat Transmission in Layered Formations," *SPE Reservoir Engineering,* vol. 5, p. 531–538, 1990.

Annexes

A1. Modified Ramey's solution

Applying Ramey's solution in successive subdomains with different characteristics requires to modify the solution and to develop a new analytical solution. Examples of application are in heterogeneous formations with different type of rocks or in cases where the geothermal gradient is not uniform across the domain. We consider here a domain which includes three subdomains with different geological properties as in Figure 35. The parameter Λ includes the heat capacity and g_T is the thermal gradient.

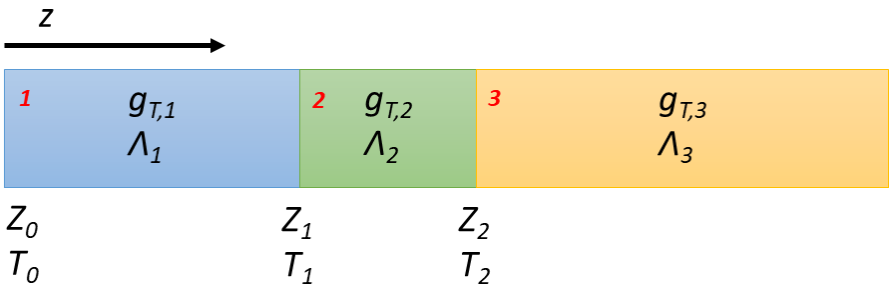

Figure 35. Subdomains with different properties for developing the modified Ramey solution.

Ramey's general solution which can be applied in each *k* subdomain is:

$$T_f(z,t) = T_e(z = Z_{k-1}) + g_{T,k}(z - Z_{k-1}) - g_{T,k}\Lambda_k + C_k e^{-\frac{z}{\Lambda_k}}, \quad \text{for } z \geq Z_{k-1} \tag{47}$$

where T_e is the initial temperature of the domain, C is an integral constant which can be found by applying the initial or boundary conditions and Z_{k-1} is the lower border of the subdomain k, with $Z_0 = 0$.

For the 1st domain with $Z_0 = 0$, the inlet fluid temperature is equal to the known T_0, and the Eq. (47) gives:

$$C_1 = T_0 - T_e(z = 0) + g_{T,1}\Lambda_1 \tag{48}$$

Thus, for the 1st domain:

$$T_f(z,t) = T_e(z = 0) + g_{T,1}z - g_{T,1}\Lambda_1 + \left[T_0 - T_e(z = 0) + g_{T,1}\Lambda_1\right]e^{-\frac{z}{\Lambda_k}} \tag{49}$$

Application of Eq. (47) on the 2nd domain results in:

$$T_f(z,t) = T_e(z = Z_1) + g_{T,2}(z - Z_1) - g_{T,2}\Lambda_2 + C_2 e^{-\frac{z}{\Lambda_2}} \tag{50}$$

The initial temperature of the domain is at Z_1:

$$T_e(z = Z_1) = T_e(z = 0) + g_{T,1}Z_1 \tag{51}$$

At the border $z = Z_1$, the fluid temperature can be found from Eq. (49) of the 1st domain and it is equal to $T_f(z = Z_1, t)$ or T_1. Thus, Eq. (50) together with Eq. (51) gives:

$$\begin{aligned} T_e(z = 0) + g_{T,1}Z_1 - g_{T,2}\Lambda_2 + C_2 e^{-\frac{Z_1}{\Lambda_2}} = T_1 \Rightarrow C_2 \\ = \left[T_1 - T_e(z = 0) - g_{T,1}Z_1 + g_{T,2}\Lambda_2\right]e^{\frac{Z_1}{\Lambda_2}} \end{aligned} \tag{52}$$

Similarly, for the 3rd domain, Eq. (47) gives:

$$T_f(z,t) = T_e(z = Z_2) + g_{T,3}(z - Z_2) - g_{T,3}\Lambda_3 + C_3 e^{-\frac{z}{\Lambda_3}} \quad (53)$$

with:

$$T_e(z = Z_2) = T_e(z = 0) + g_{T,1}Z_1 + g_{T,2}Z_2 \quad (54)$$

At $z = Z_2$, Eq. (53) allows the calculation of the constant C_3:

$$\begin{aligned} T_e(z=0) + g_{T,1}Z_1 + g_{T,2}Z_2 - g_{T,3}\Lambda_3 + C_3 e^{-\frac{Z_2}{\Lambda_3}} = T_2 \Rightarrow C_3 \\ = \left[T_2 - T_e(z=0) - g_{T,1}Z_1 - g_{T,2}Z_2 + g_{T,3}\Lambda_3\right] e^{\frac{Z_2}{\Lambda_3}} \end{aligned} \quad (55)$$

Following the above process, the calculation of the fluid temperature of the any domain is possible. The below table includes the above equations for 3 domains, and the generalization for the *k* domain.

Table 17.The modified Ramey's solution for multidomain.

Domain, k	Equation, $T_f(z,t)$	Constant, C_k
1	$T_e(z=0) + g_{T,1}z - g_{T,1}\Lambda_1 + C_1 e^{-\frac{z}{\Lambda_k}}$	$T_f(z=0,t) - T_e(z=0) + g_{T,1}\Lambda_1$
2	$T_e(z=0) + g_{T,1}Z_1 + g_{T,2}(z - Z_1) - g_{T,2}\Lambda_2 + C_2 e^{-\frac{z-Z_1}{\Lambda_2}}$	$T_f(z=Z_1,t) - T_e(z=0) - g_{T,1}Z_1 + g_{T,2}\Lambda_2$
3	$T_e(z=0) + g_{T,1}Z_1 + g_{T,2}Z_2 + g_{T,3}(z - Z_2) - g_{T,3}\Lambda_3 + C_3 e^{-\frac{z-Z_2}{\Lambda_3}}$	$T_f(z=Z_2,t) - T_e(z=0) - g_{T,1}Z_1 - g_{T,2}Z_2 + g_{T,3}\Lambda_3$
k	$T_e(z=0) + \sum_{k=1,k>1}^{k-1} g_{T,k}Z_k + g_{T,k}(z - Z_{k-1}) - g_{T,k}\Lambda_k + C_k e^{-\frac{z-Z_{k-1}}{\Lambda_k}}$	$T_f(z=Z_{k-1},t) - T_e(z=0) - \sum_{k=1,k>1}^{k-1} g_{T,k}Z_k + g_{T,k}\Lambda_k$

Three examples of applying the above general equation are presented hereafter. In the first example, which corresponds to the simulated case b (Figure 3), there are two subdomains with the same properties but the geothermal gradient on the 2nd subdomain in zero. In the second example (case c, Figure 4), the two domains have the same gradient, but different thermal conductivity. Finally, in the third example (case d, Figure 4) the two subdomains have different gradient and conductivity.

Table 18. Examples of applying the modified Ramey solution

Example	Description	Equations
case b	2 subdomains $\Lambda_1 = \Lambda_2 = \Lambda$, $g_{T,1}$, $g_{T,2} = 0$	$T_f(z \le Z_1,t) = T_e(z=0) + g_{T,1}z - g_{T,1}\Lambda + C_1 e^{-\frac{z}{\Lambda}}$ $C_1 = T_f(z=0,t) - T_e(z=0) + g_{T,1}\Lambda$ $T_f(z > Z_1,t) = T_e(z=0) + g_{T,1}Z_1 + C_2 e^{-\frac{z-Z_1}{\Lambda}}$ $C_2 = T_f(z=Z_1,t) - T_e(z=0) - g_{T,1}Z_1$
case c	2 subdomains Λ_1, Λ_2, $g_{T,1} = g_{T,2} = g_T$	$T_f(z \le Z_1,t) = T_e(z=0) + g_T z - g_T\Lambda_1 + C_1 e^{-\frac{z}{\Lambda_1}}$ $C_1 = T_f(z=0,t) - T_e(z=0) + g_T\Lambda_1$ $T_f(z > Z_1,t) = T_e(z=0) + g_T z - g_T\Lambda_2 + C_2 e^{-\frac{z-Z_1}{\Lambda_2}}$ $C_2 = T_f(z=Z_1,t) - T_e(z=0) - g_T Z_1 + g_T\Lambda_2$
Case d	2 subdomains Λ_1, Λ_2, $g_{T,1}$, $g_{T,2}$	$T_f(z \le Z_1,t) = T_e(z=0) + g_{T,1}z - g_{T,1}\Lambda_1 + C_1 e^{-\frac{z}{\Lambda_1}}$ $C_1 = T_f(z=0,t) - T_e(z=0) + g_{T,1}\Lambda_1$ $T_f(z > Z_1,t) = T_e(z=0) + g_{T,1}Z_1 + g_{T,2}(z - Z_1) - g_{T,2}\Lambda_2 + C_2 e^{-\frac{z-Z_1}{\Lambda_2}}$ $C_2 = T_f(z=Z_1,t) - T_e(z=0) - g_{T,1}Z_1 + g_{T,2}\Lambda_2$

A2. Software mapping

Software	Purpose	Equations	Fluids	Input	Output	Type of use	User
COMSOL	Heat and fluid flow reservoir-wellbore numerical modelling. The reservoir is assumed to be a porous, permeable, or impermeable medium and a small number of discrete fracture planes can be incorporated. Wellbore flow/heat transfer are coupled weakly through boundary conditions in separate simulations.	Conductive and advective time-dependent heat transfers in the reservoir and wellbore. Darcy flow constitutive model in the reservoir. 2D radially symmetric wellbore flow modelled with laminar flow module based on the Navier-Stokes equations. The software can couple multiple physics including geomechanics, heat and fluid flow.	Water has been used as working fluid so far	Rock properties (thermal and hydraulic), fluid properties, geometry of the well and reservoir, fluid rates. Initial pressure and temperature.	Production temperature, and pressure in the reservoir	License required	VITO
GWellFM	Hydrodynamic (single- or multiphase), thermodynamic (EoS) and heat transfer modelling. Wellbore fluid flow, Wellbore/formation heat transfer.	1D steady-state mass, momentum, and enthalpy balances in the wellbore, 2D transient heat transfer in the formation. Single or dual pipe (coaxial well), production or injection, co-current or counter-current flow.	Water, CO_2, or any fluid (mixture) with a proper EoS.	Detailed completion, fluid rates, initial T & P, solid thermal properties.	Spatial and temporal evolution of fluid pressure, temperature, properties, and composition	IFPEN's in-house tool	IFPEN

GTW	A simulator for borehole coaxial heat exchangers.	1D steady-state one-phase mass, momentum, and energy balance in the heat exchanger. Radial and vertical heat conduction in cylinder coordinates in the rock.	Water with constant properties. Pressure- and temperature-dependent fluid properties can be provided in tables.	Rock properties (thermal and hydraulic), fluid properties, the geometry of the well and reservoir, and fluid rates. Initial pressure and temperature.	Pressure and temperature of the working fluid in the heat exchanger at provided times. The temperature in the rock at provided times.	IFE in-house. Plans to release it under the GPL license.	IFE

A3. Case a: Vertical injection well

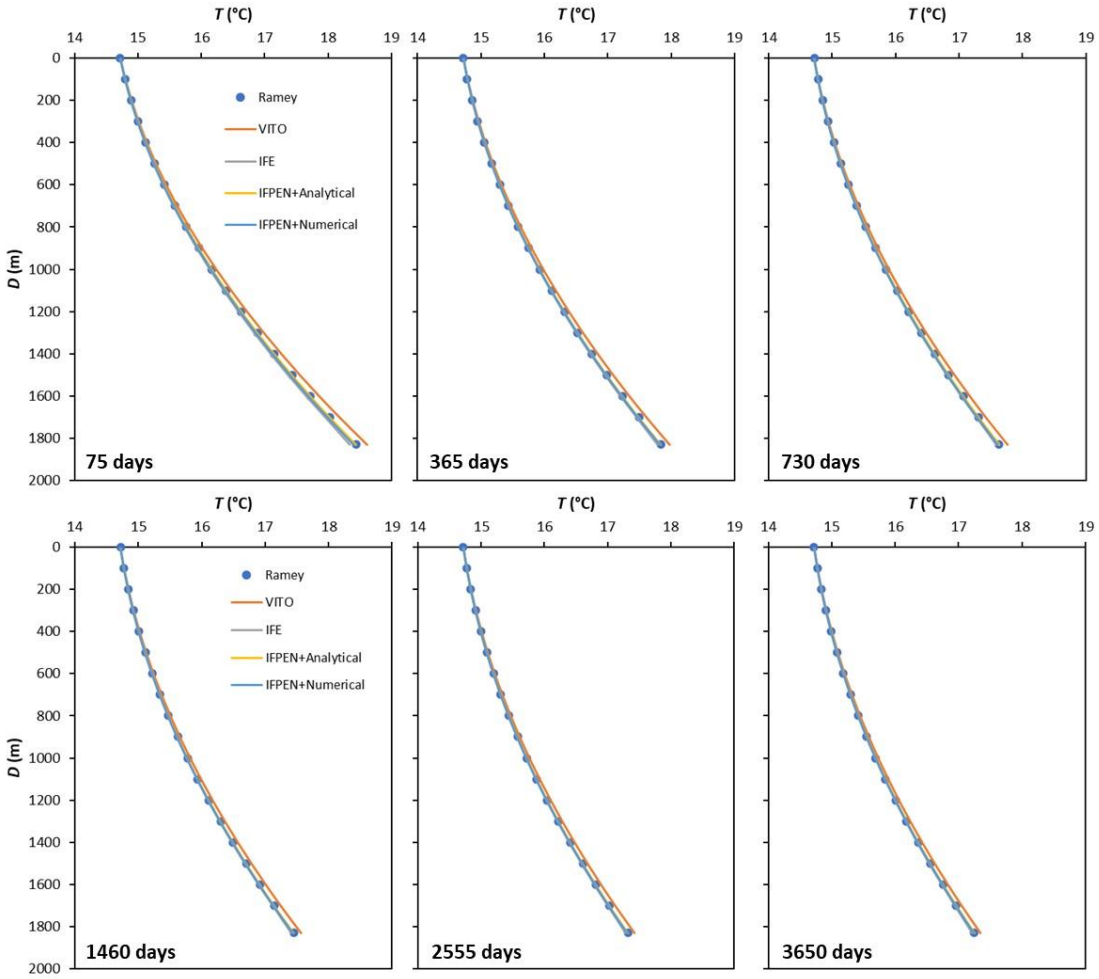

Figure 36. Comparison of fluid temperature along the well for case a at different times.

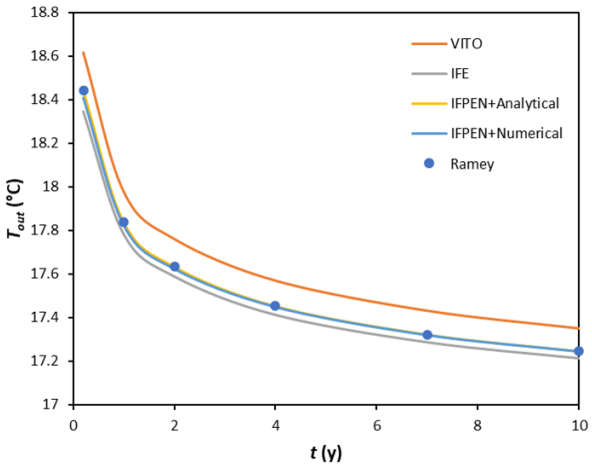

Figure 37. Comparison of the temporal evolution of the outlet temperature of the well for case a.

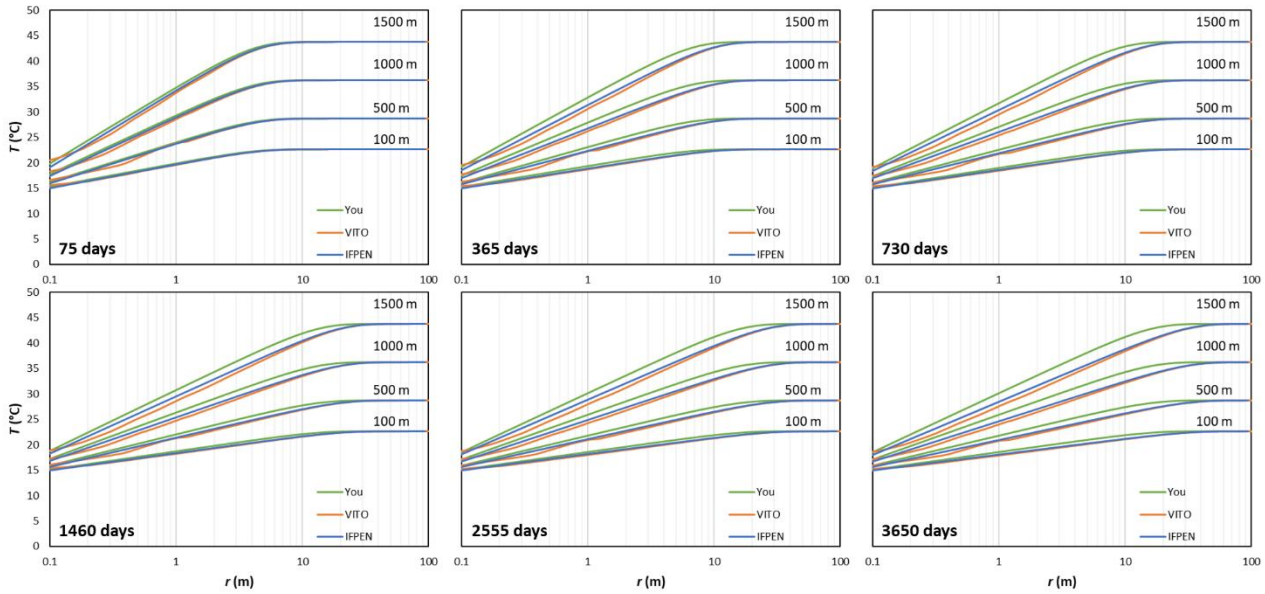

Figure 38. Comparison of temperature profiles in the formation at various depths and times for case a between IFPEN's model and You's analytical model.

Table 19. Hardware specificities and numerical details for simulating case a.

User	Simulator	**Hardware**	**Setting up**	**Discretization**	**Time step**	**Total number of** time steps	**Simulation time [min]**
VITO	COMSOL	CPU Intel i7-12850HX @ 2.10 GHz RAM 32 GB	Easy, through Pipe flow module, no major control on mesh creation	≈760000 tetrahedral cells 1 m cell size along the well	Min: 86.4 s, Max: 1296000 s	200	26,3
IFPEN	GWellFM	CPU Intel i7-8850H @ 2.60 GHz RAM 16 GB	Easy	73 axial cells regular sized, 50 radial cells with geometric progression and 0.01 m minimum size	Min: 3600 s, Max: 2592000 s	160	42
IFE	GTW	CPU Intel i7-11850H @ 2.50GHz RAM 15 GB	Easy	2-D grid of cylinder coordinates, 50 cells radially and 253 cells vertically	Min 1 day Max 100 days	58	<1

A4. Case b: Horizontal injection well

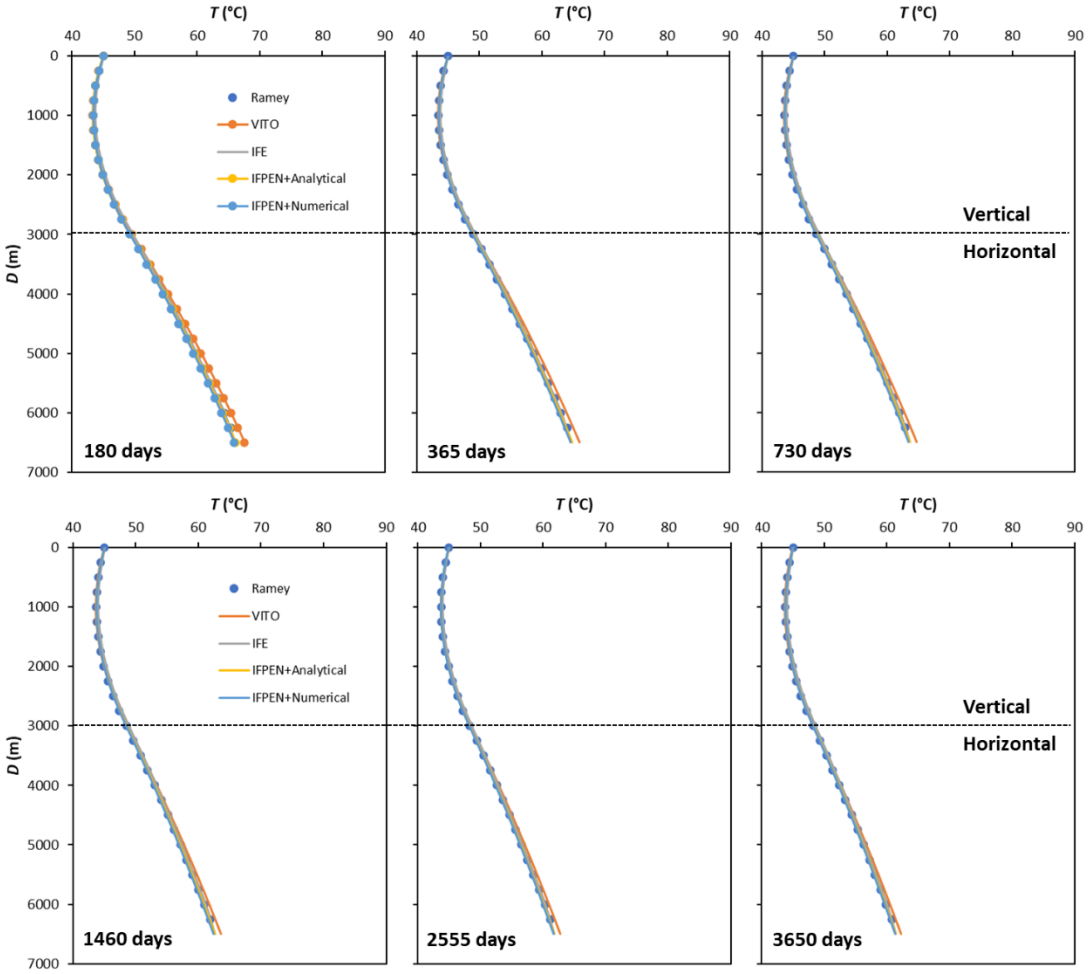

Figure 39. Comparison of fluid temperature along the well for case b at different times.

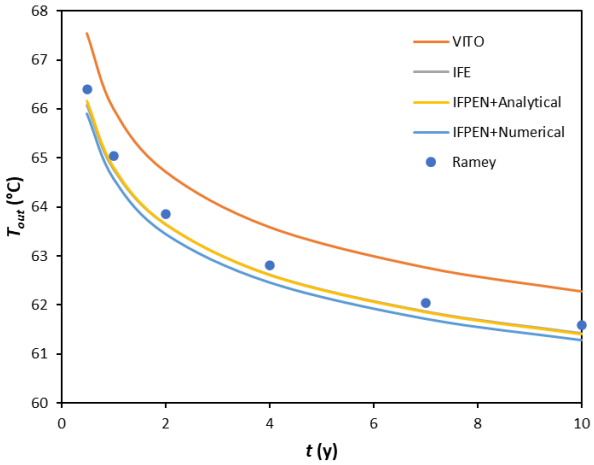

Figure 40. Comparison of the temporal evolution of the outlet temperature of the well for case b.

Table 20. Hardware specificities and numerical details for simulating case b.

User	Simulator	**Hardware**	**Setting up**	**Discretization**	**Time step**	**Total number of** time steps	**Simulation time [min]**
VITO	COMSOL	CPU Intel i7-12850HX @ 2.10 GHz RAM 32 GB	Moderate, through Pipe flow module, 3D domain creation, large number of cells is needed	≈1000000 tetrahedral cells 1.5 m cell size along the well	Min: 86.4 s, Max: 1296000 s	200	27,4
IFPEN	GWellFM	CPU Intel i7-8850H @ 2.60 GHz RAM 16 GB	Easy	130 axial cells regular sized, 50 radial cells with geometric progression and 0.01 m minimum size	Min: 3600 s, Max: 2592000 s	160	93
IFE	GTW	CPU Intel i7-11850H @ 2.50GHz RAM 15 GB	Easy	2-D grid of cylinder coordinates, 50 cells radially and 68 cells vertically	Min 1 day Max 100 days	58	<1

A5. Case c: Injection well and heterogeneous formation

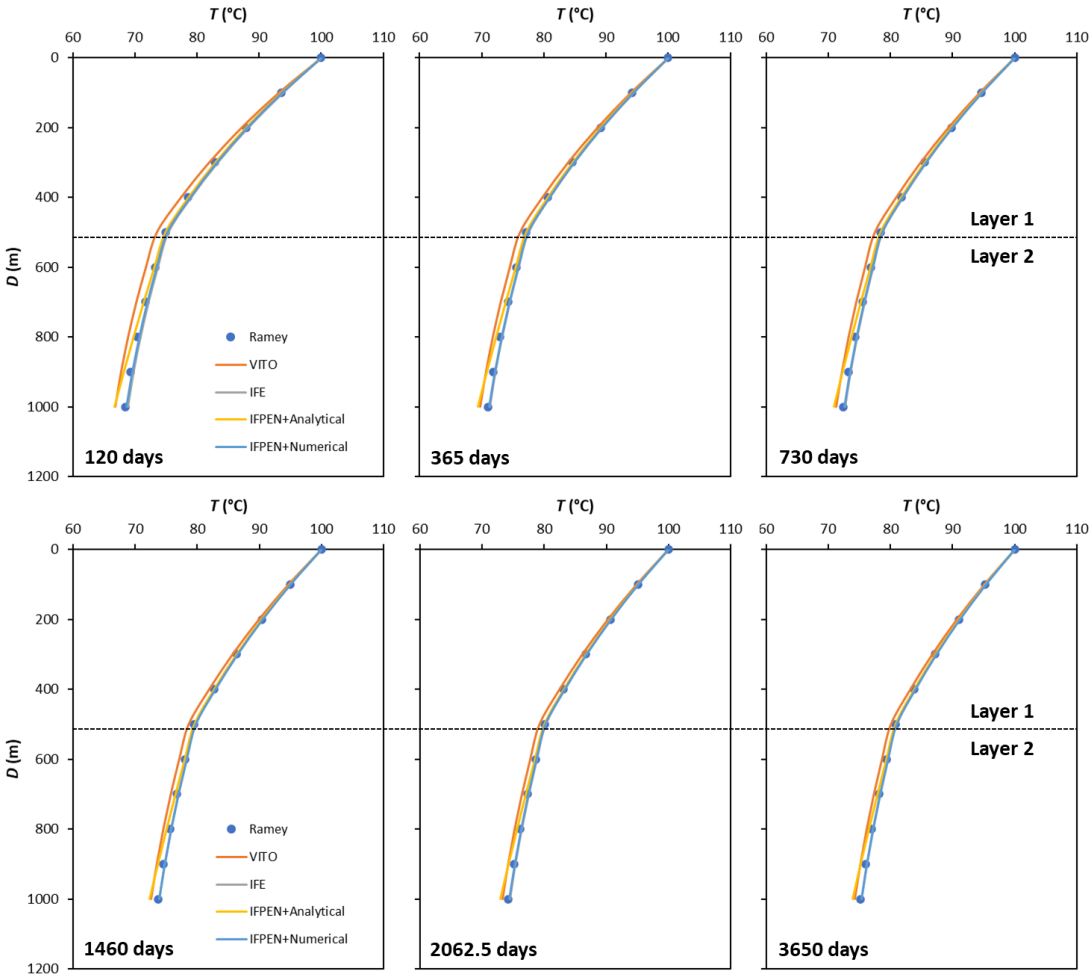

Figure 41. Comparison of fluid temperature along the well for case c at different times.

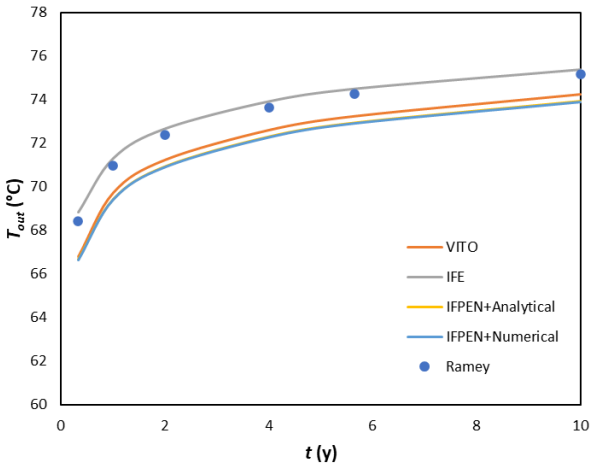

Figure 42. Comparison of the temporal evolution of the outlet temperature of the well for case c.

Table 21. Hardware specificities and numerical details for simulating case c.

User	Simulator	**Hardware**	**Setting up**	**Discretization**	**Time step**	**Total number of time steps**	**Simulation time [min]**
VITO	COMSOL	CPU Intel i7-12850HX @ 2.10 GHz RAM 32 GB	Easy, through Pipe flow module, no major control on mesh creation	≈560000 tetrahedral cells 1 m cell size along the well	Min: 86.4 s, Max: 1296000 s	200	12
IFPEN	GWellFM	CPU Intel i7-8850H @ 2.60 GHz RAM 16 GB	Easy	20 axial cells regular sized, 50 radial cells with geometric progression and 0.01 m minimum size	Min: 3600 s, Max: 2592000 s	160	10
IFE	GTW	CPU Intel i7-11850H @ 2.50GHz RAM 15 GB	Easy	2-D grid of cylinder coordinates, 50 cells radially and 203 cells vertically	Min 1 day Max 100 days	56	<1

A6. Case d: Horizontal well and heterogeneous formation

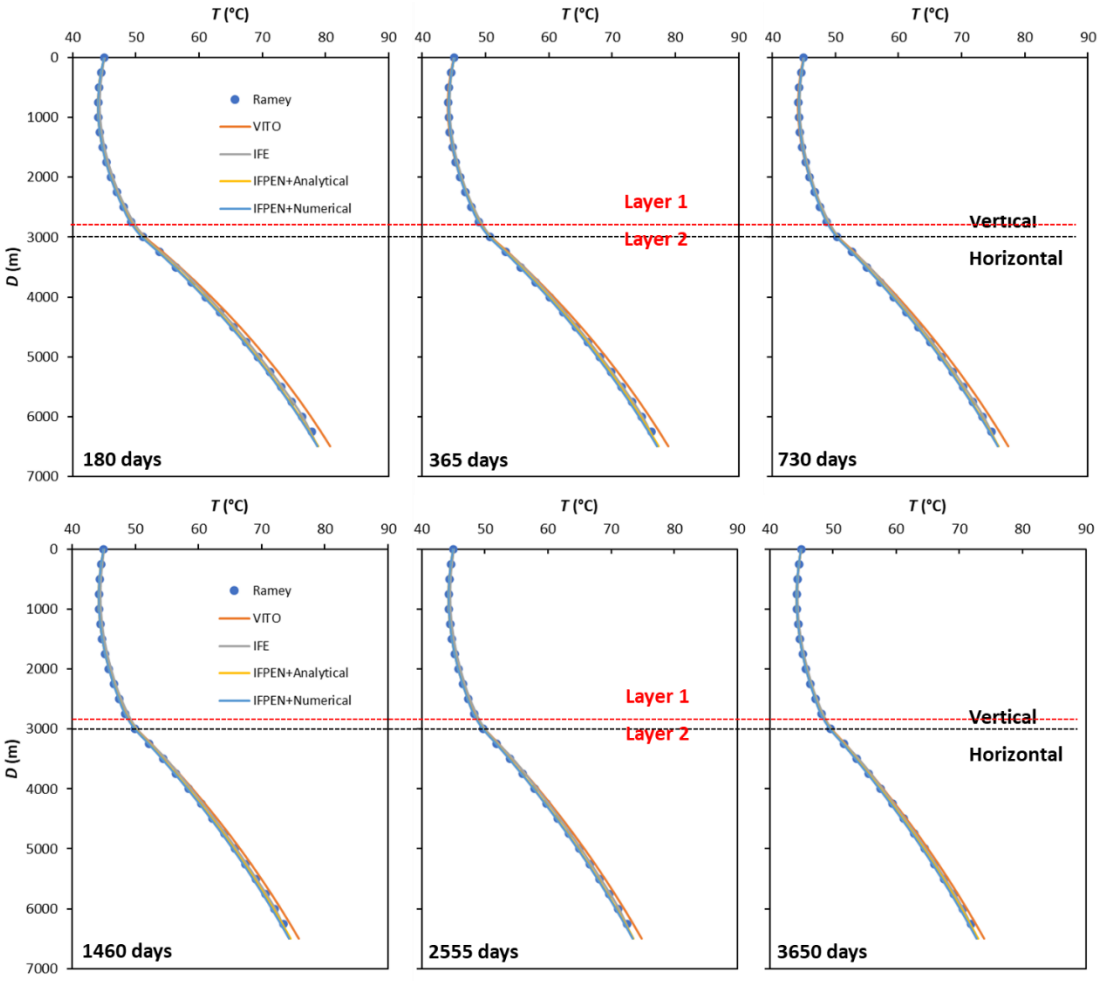

Figure 43. Comparison of fluid temperature along the well for case d at different times.

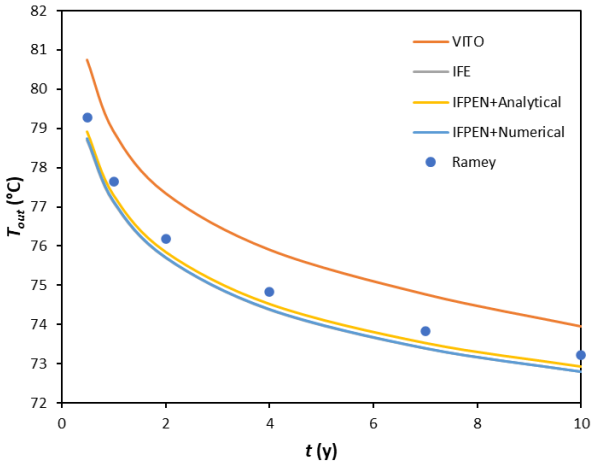

Figure 44. Comparison of the temporal evolution of the outlet temperature of the well for case d.

Table 22. Hardware specificities and numerical details for simulating case d.

User	Simulator	**Hardware**	**Setting up**	**Discretization**	**Time step**	**Total number of** time steps	**Simulation time [min]**
VITO	COMSOL	CPU Intel i7-12850HX @ 2.10 GHz RAM 32 GB	Moderate, through Pipe flow module, 3D domain creation, large number of cells is needed	≈1800000 tetrahedral cells 1 m cell size along the well	Min: 86.4 s, Max: 1296000 s	200	64
IFPEN	GWellFM	CPU Intel i7-8850H @ 2.60 GHz RAM 16 GB	Easy	130 axial cells regular sized, 50 radial cells with geometric progression and 0.01 m minimum size	Min: 3600 s, Max: 2592000 s	160	70
IFE	GTW	CPU Intel i7-11850H @ 2.50GHz RAM 15 GB	Easy	2-D grid of cylinder coordinates, 50 cells radially and 73 cells vertically	Min 1 day Max 100 days	56	<1

A7. Case e: Vertical coaxial closed well

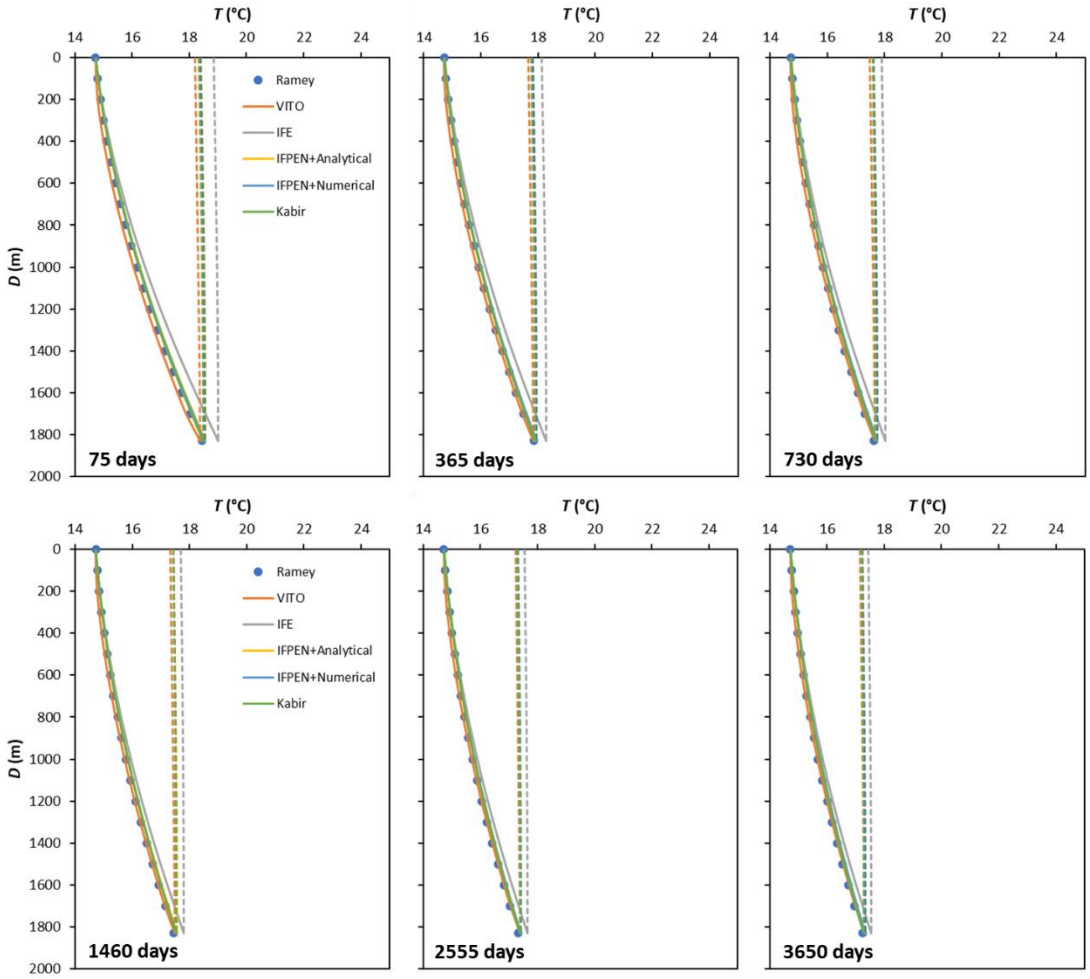

Figure 45. Comparison of fluid temperature along the well for case e at different times.

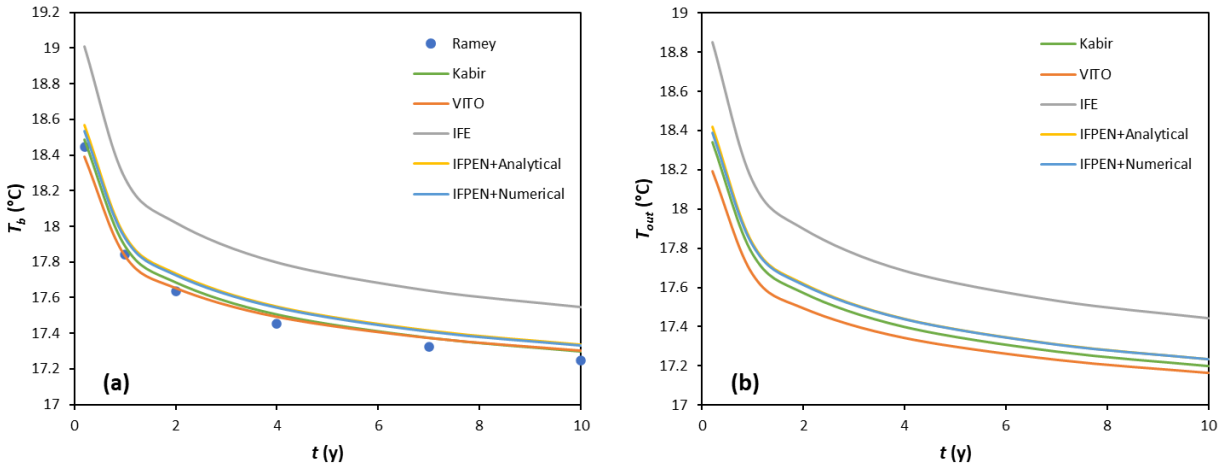

Figure 46. Comparison of the temporal evolution of (a) the temperature at the bottom of the annulus part and (b) the outlet temperature of the well for case e.

Table 23. Hardware specificities and numerical details for simulating case e.

User	Simulator	**Hardware**	**Setting up**	**Discretization**	**Time step**	**Total number of** time steps	**Simulation time [min]**
VITO	COMSOL	CPU Intel i7-12850HX @ 2.10 GHz RAM 32 GB	Moderate, through flow and heat in porous media modules, imposing Nusselt number, 3D domain creation	≈220000 radial cells 1.5 m cell size along the well	Min: 86.4 s, Max: 1296000 s	200	42
IFPEN	GWellFM	CPU Intel i7-8850H @ 2.60 GHz RAM 16 GB	Easy	73 axial cells regular sized, 50 radial cells with geometric progression and 0.01 m minimum size	Min: 3600 s, Max: 2592000 s	160	40
IFE	GTW	CPU Intel i7-11850H @ 2.50GHz RAM 15 GB	Easy	2-D grid of cylinder coordinates, 50 cells radially and 253 cells vertically	Min 1 day Max 100 days	58	<1

A8. Case f: Horizontal coaxial closed well

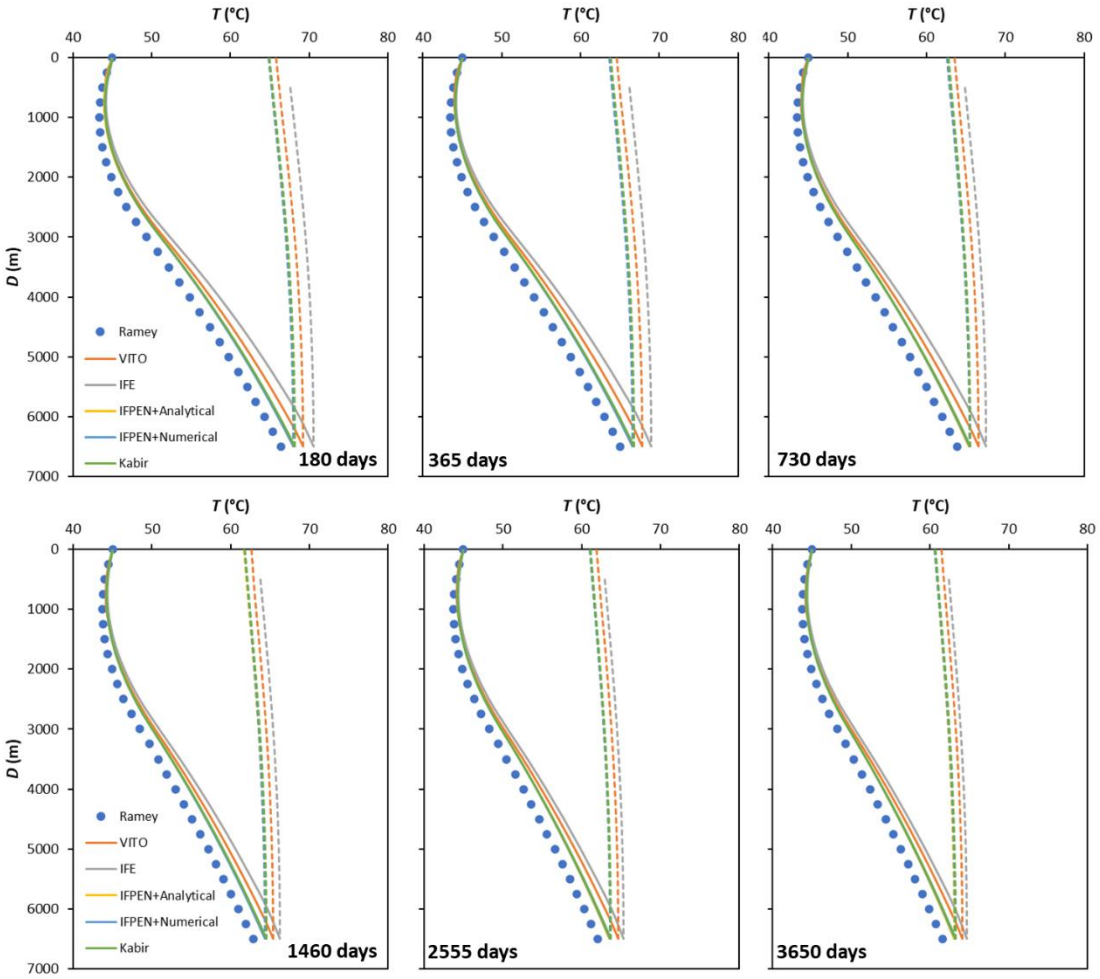

Figure 47. Comparison of fluid temperature along the well for case f at different times.

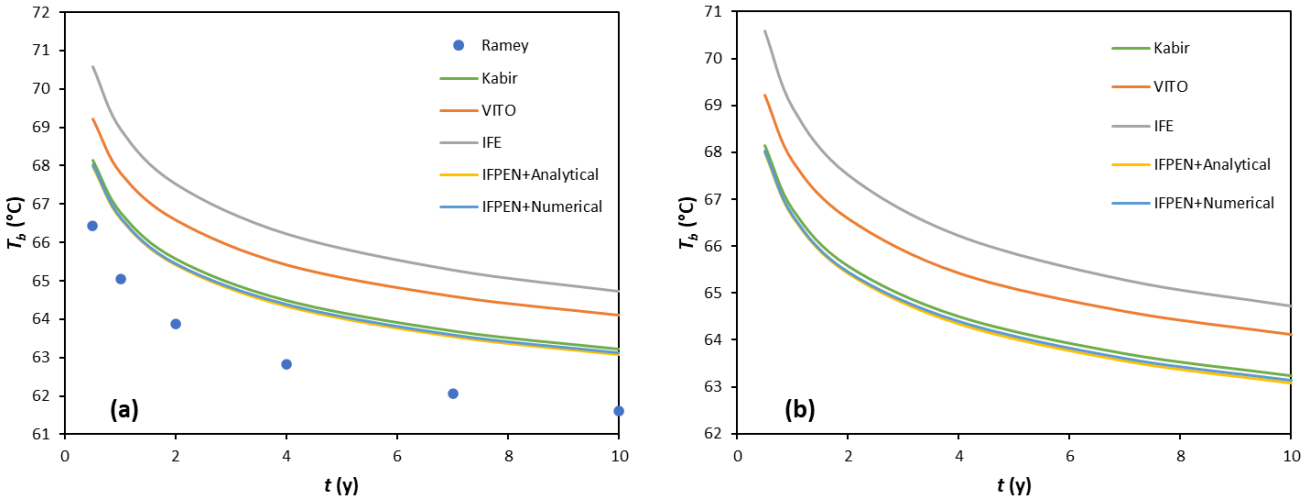

Figure 48. Comparison of the temporal evolution of (a) the temperature at the bottom of the annulus part and (b) the outlet temperature of the well for case f.

Table 24. Hardware specificities and numerical details for simulating case f.

User	Simulator	**Hardware**	**Setting up**	**Discretization**	**Time step**	**Total number of** time steps	**Simulation time [min]**
VITO	COMSOL	CPU Intel i7-12850HX @ 2.10 GHz RAM 32 GB	Moderate, through flow and heat in porous media modules, imposing Nusselt number, 3D domain creation	≈365000 radial cells 10 m cell size along the well	Min: 86.4 s, Max: 1296000 s	259	224
IFPEN	GWellFM	CPU Intel i7-8850H @ 2.60 GHz RAM 16 GB	Easy	130 axial cells regular sized, 50 radial cells with geometric progression and 0.01 m minimum size	Min: 7200 s, Max: 2592000 s	158	87
IFE	GTW	CPU Intel i7-11850H @ 2.50GHz RAM 15 GB	Easy	2-D grid of cylinder coordinates, 50 cells radially and 68 cells vertically	Min 1 day Max 100 days	58	<1

A9. Case g: Cemented vertical coaxial closed well

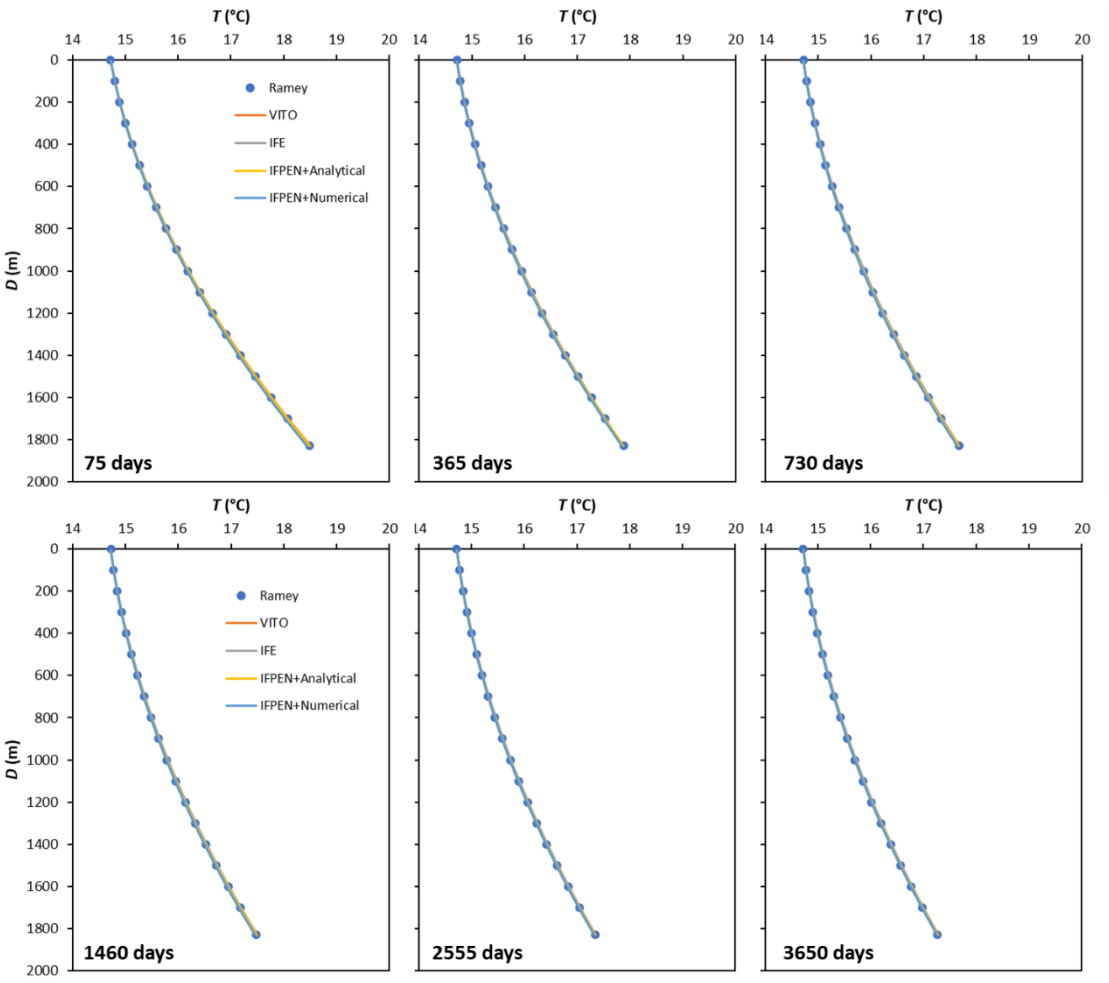

Figure 49. Comparison of fluid temperature along the well for case g at different times.

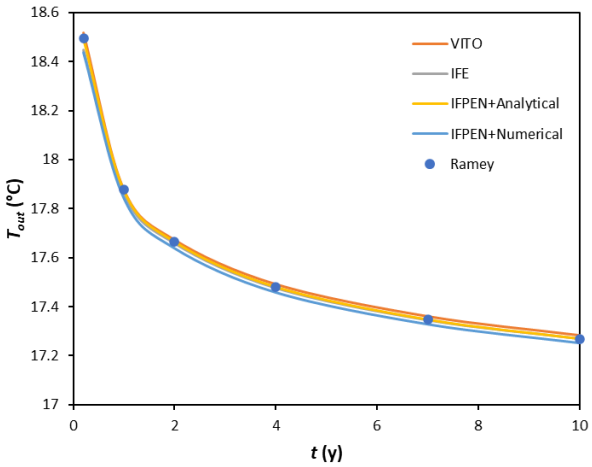

Figure 50. Comparison of the temporal evolution of the outlet temperature of the well for case g.

Table 25. Hardware specificities and numerical details for simulating case g.

User	Simulator	**Hardware**	**Setting up**	**Discretization**	**Time step**	**Total number of time steps**	**Simulation time [min]**
VITO	COMSOL	CPU Intel i7-12850HX @ 2.10 GHz RAM 32 GB	Easy, through Pipe flow module, no major control on mesh creation	≈760000 tetrahedral cells 1 m cell size along the well	Min: 86.4 s, Max: 1296000 s	200	28
IFPEN	GWellFM	CPU Intel i7-8850H @ 2.60 GHz RAM 16 GB	Easy	73 axial cells regular sized, 50 radial cells with geometric progression and 0.01 m minimum size	Min: 3600 s, Max: 2592000 s	160	55
IFE	GTW	CPU Intel i7-11850H @ 2.50GHz RAM 15 GB	Easy	2-D grid of cylinder coordinates, 50 cells radially and 253 cells vertically	Min 1 day Max 100 days	58	<1

A10. Case h: Partially cemented vertical coaxial closed well

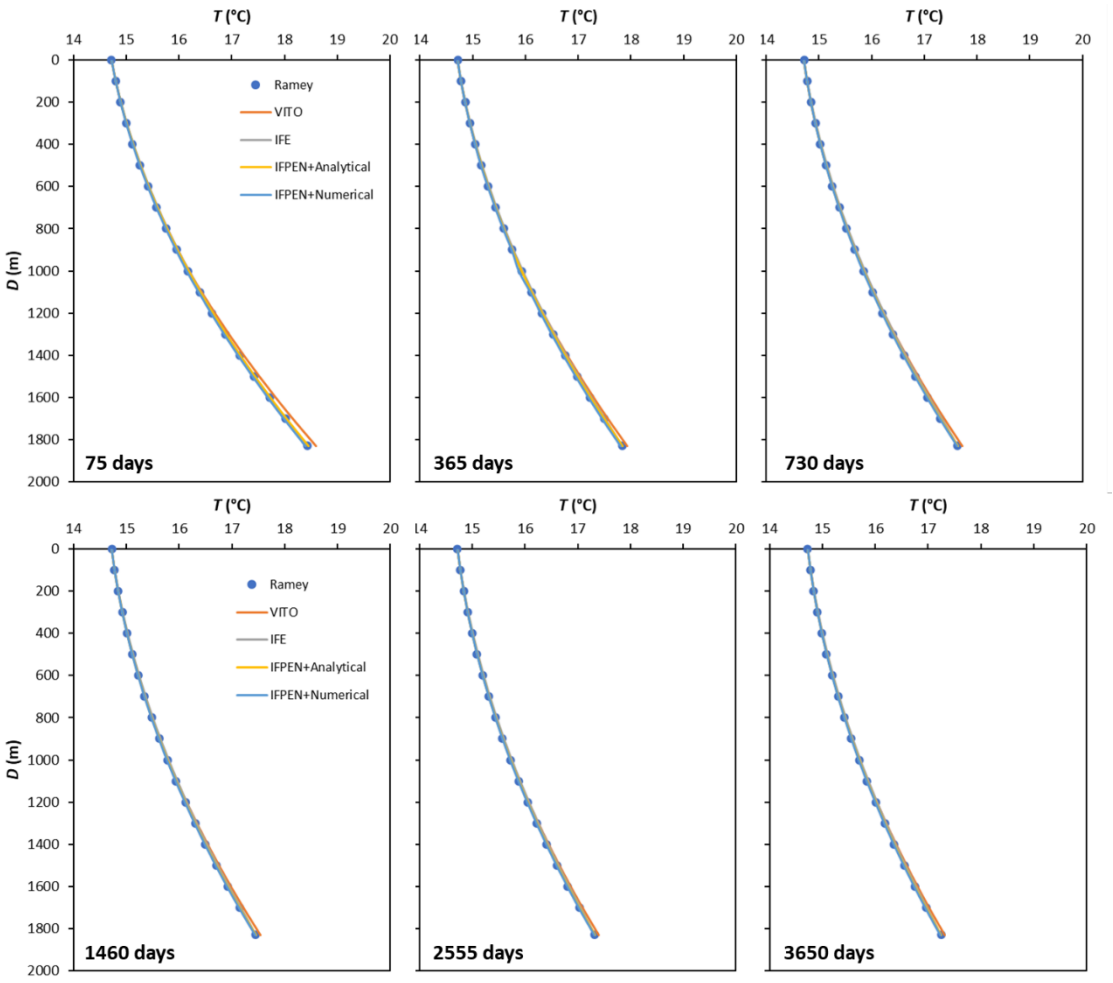

Figure 51. Comparison of fluid temperature along the well for case h at different times.

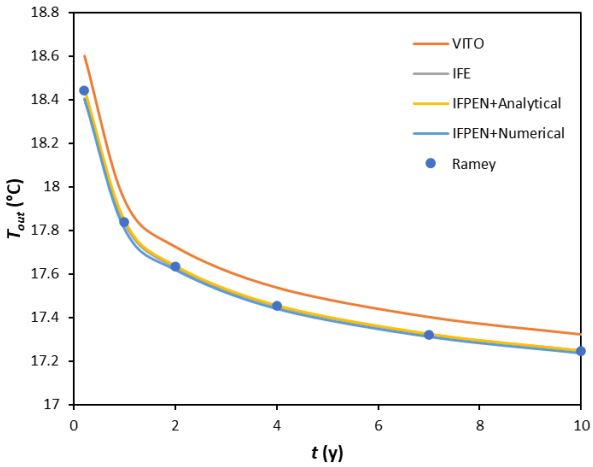

Figure 52. Comparison of the temporal evolution of the outlet temperature of the well for case h.

Table 26. Hardware specificities and numerical details for simulating case h.

User	Simulator	**Hardware**	**Setting up**	**Discretization**	**Time step**	**Total number of** time steps	**Simulation time [min]**
VITO	COMSOL	CPU Intel i7-12850HX @ 2.10 GHz RAM 32 GB	Easy, through Pipe flow module, no major control on mesh creation	≈760000 tetrahedral cells 1 m cell size along the well	Min: 86.4 s, Max: 1296000 s	200	27.5
IFPEN	GWellFM	CPU Intel i7-8850H @ 2.60 GHz RAM 16 GB	Easy	73 axial cells regular sized, 50 radial cells with geometric progression and 0.01 m minimum size	Min: 3600 s, Max: 2592000 s	160	96
IFE	GTW	CPU Intel i7-11850H @ 2.50GHz	Easy	Regual grid in cylinder coordinates 50x183=9150 cells	Min 1 day Max 100 days	58	1

A11. Cases e1-e2: Impact of central tubing thermal conductivity on coaxial closed wells

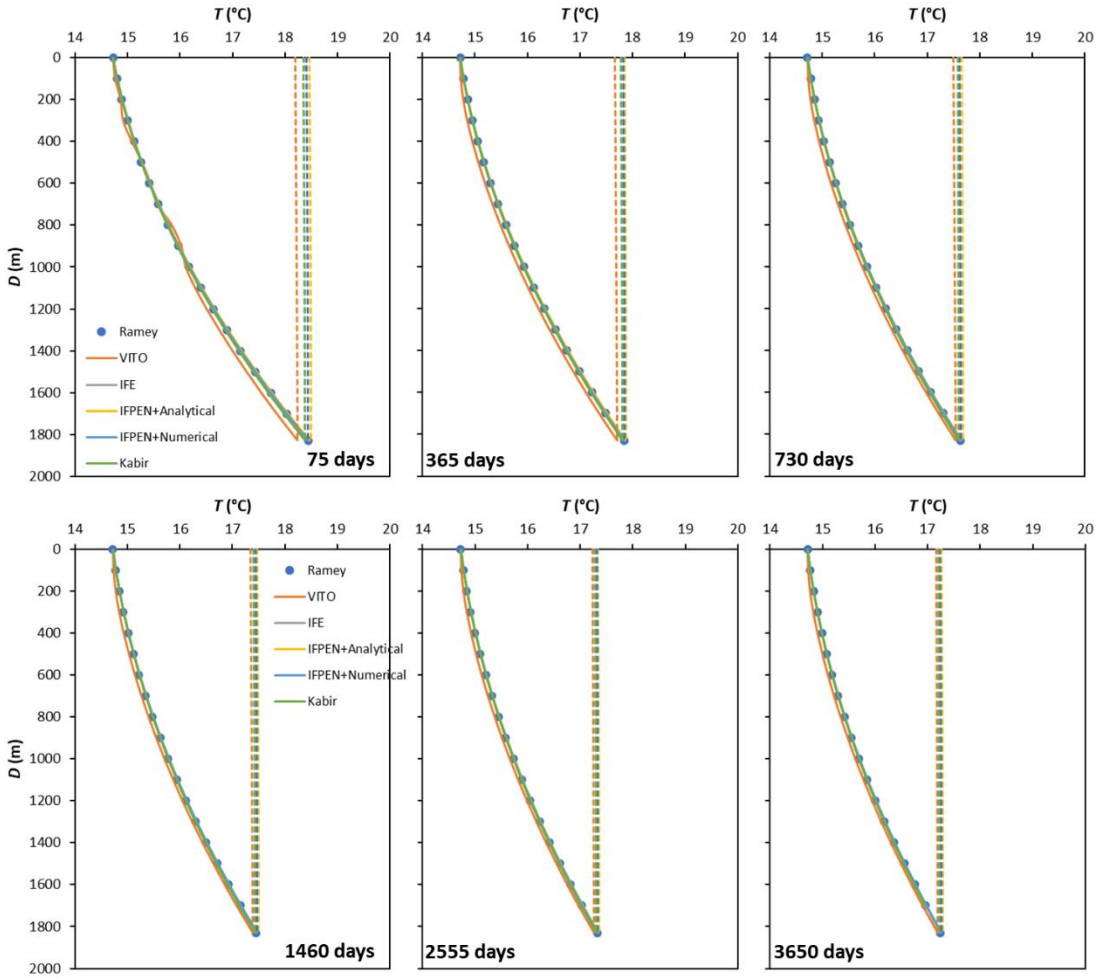

Figure 53. Comparison of fluid temperature along the well for case e1 at different times.

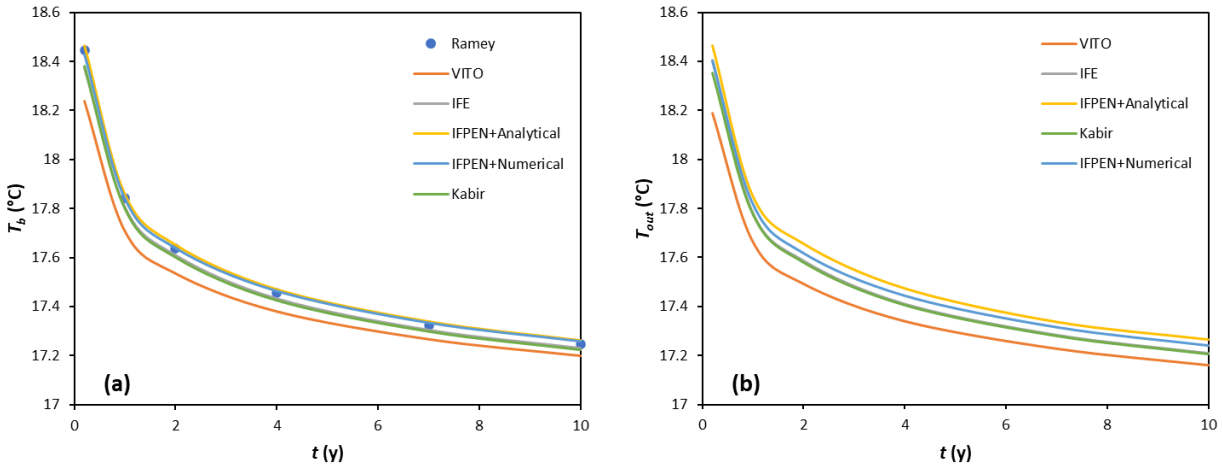

Figure 54. Comparison of the temporal evolution of (a) the temperature at the bottom of the annulus part and (b) the outlet temperature of the well for case e1.

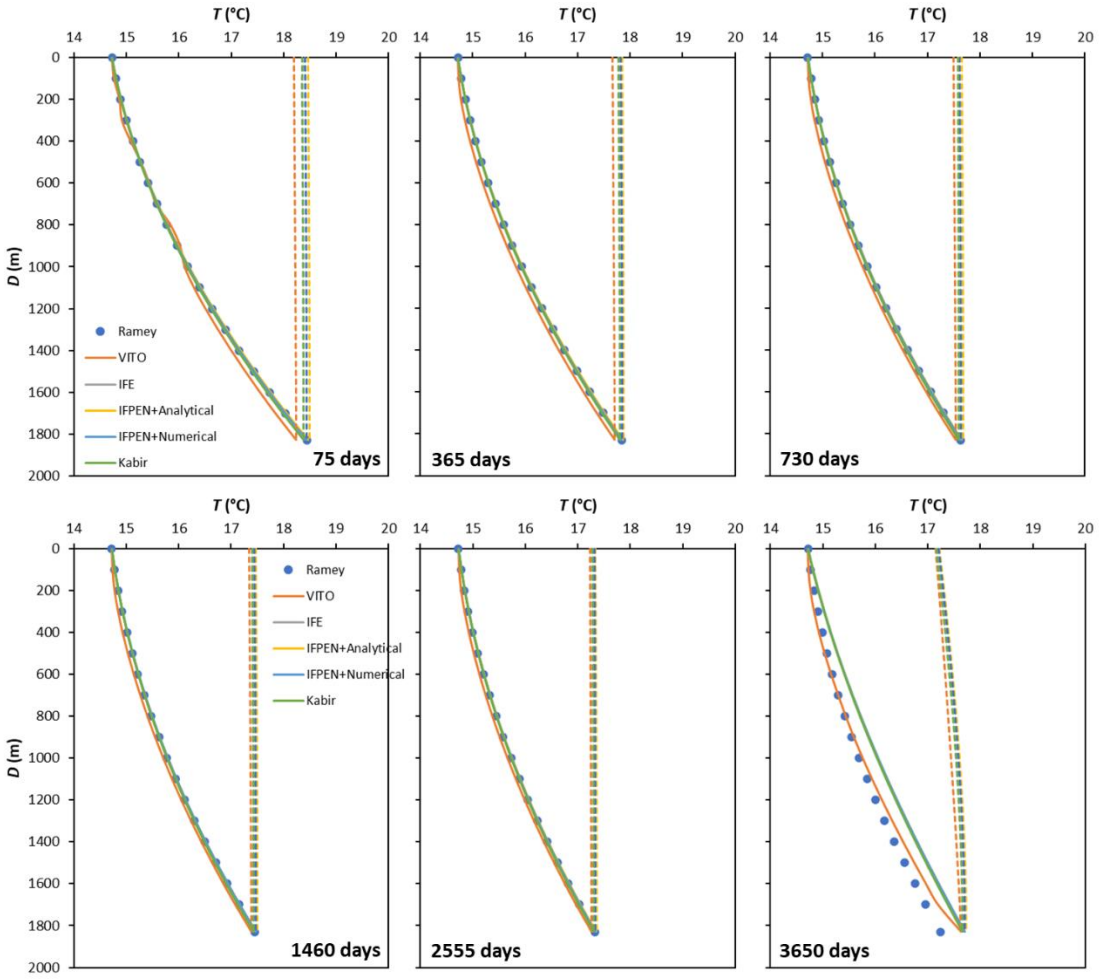

Figure 55. Comparison of fluid temperature along the well for case e2 at different times.

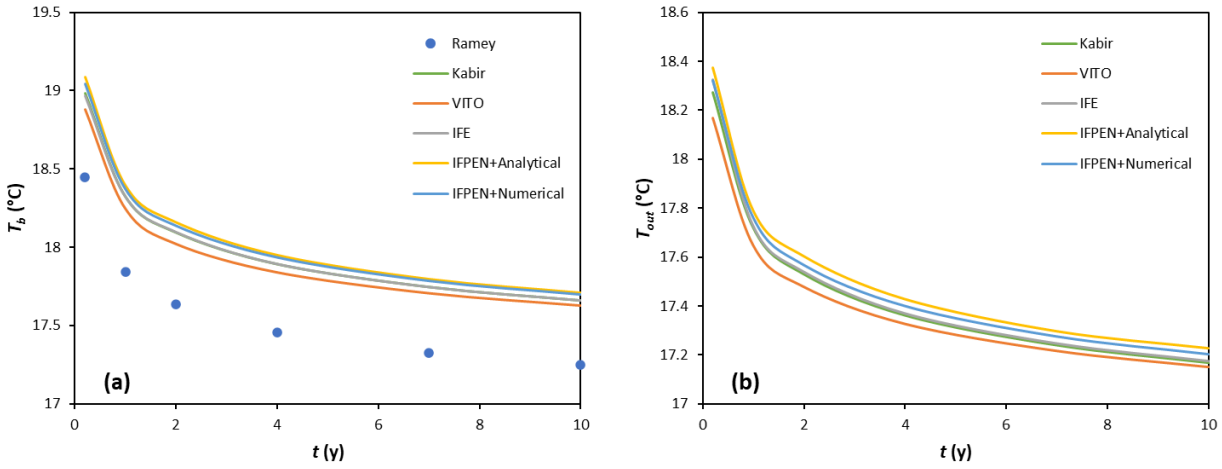

Figure 56. Comparison of the temporal evolution of (a) the temperature at the bottom of the annulus part and (b) the outlet temperature of the well for case e2.

A12. Cases e3-e4-e5: Impact of injection flow rate on coaxial closed wells

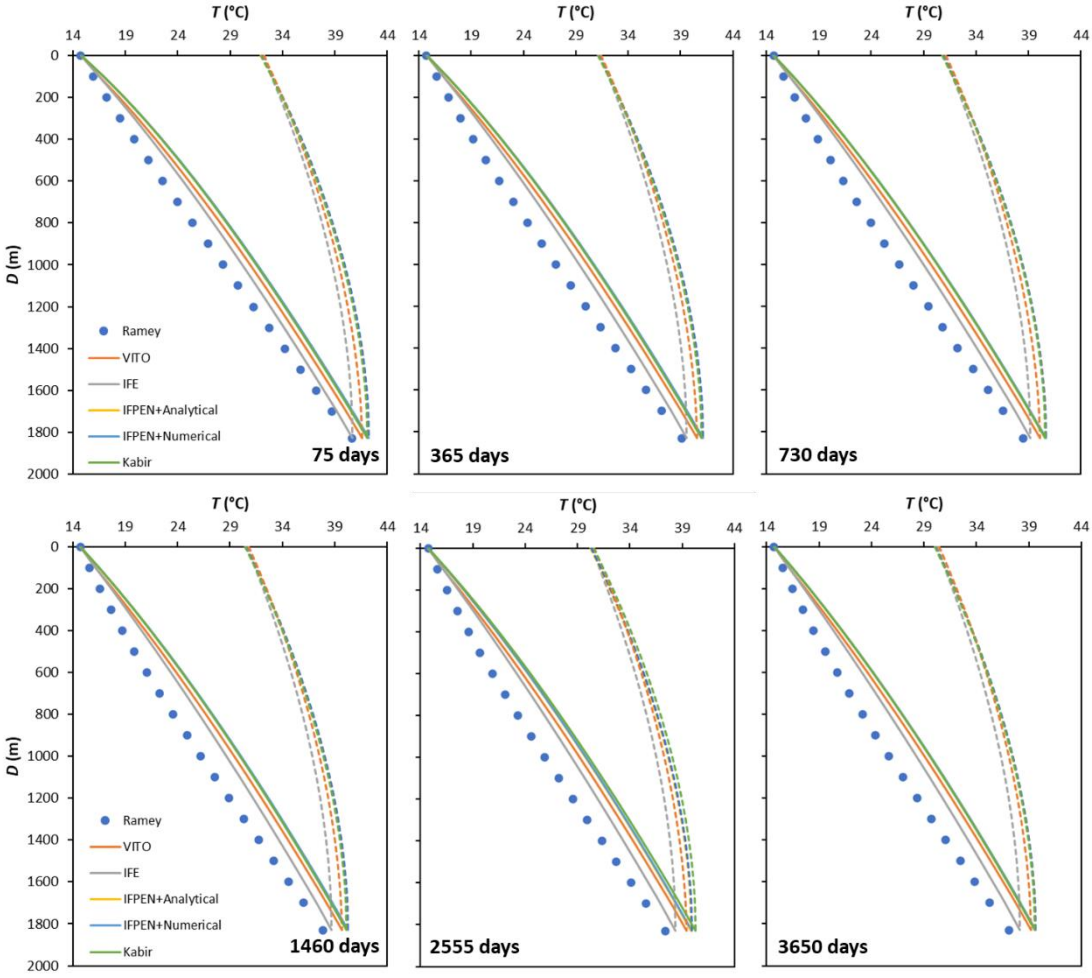

Figure 57. Comparison of fluid temperature along the well for case e3 at different times.

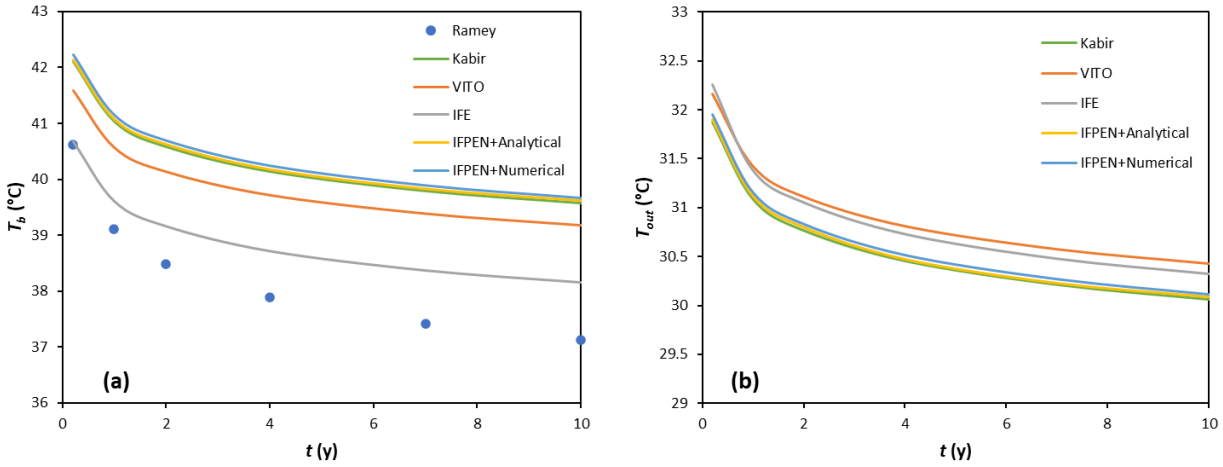

Figure 58. Comparison of the temporal evolution of (a) the temperature at the bottom of the annulus part and (b) the outlet temperature of the well for case e3.

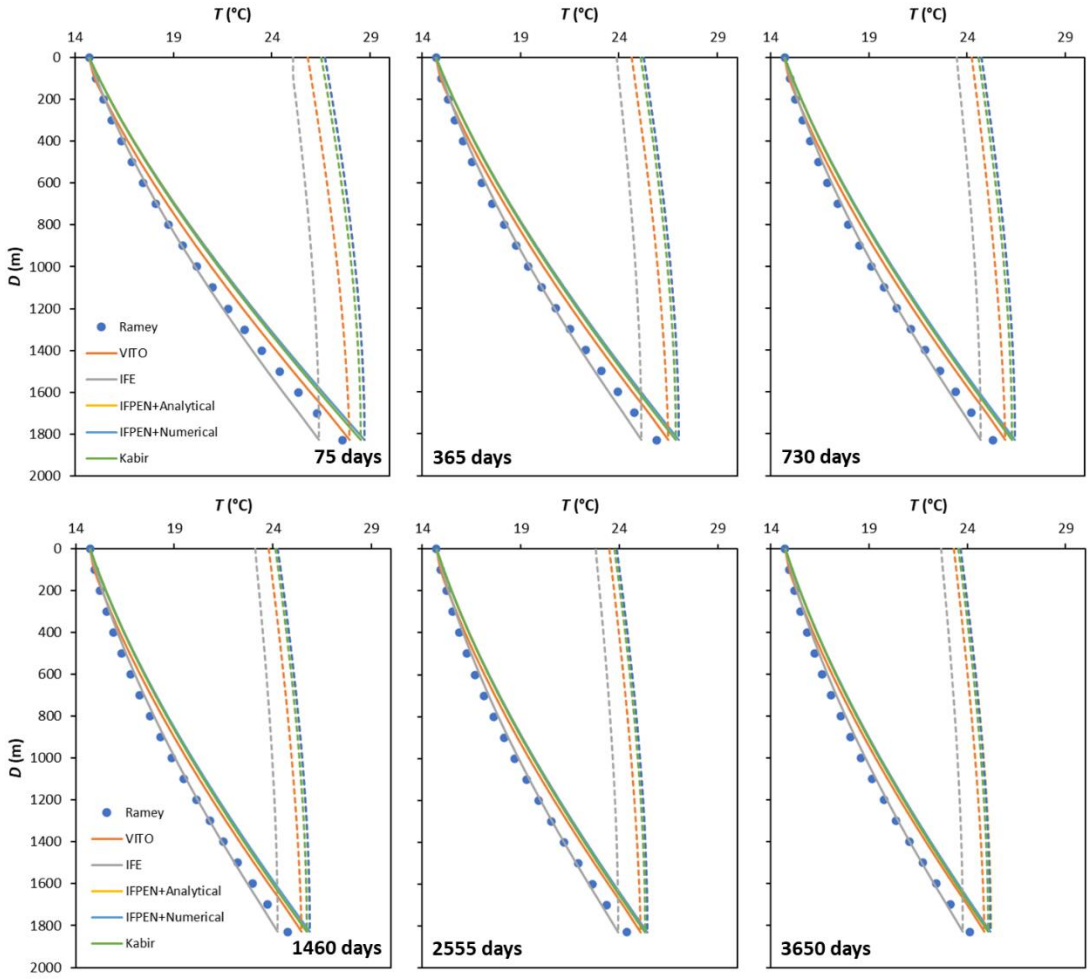

Figure 59. Comparison of fluid temperature along the well for case e4 at different times.

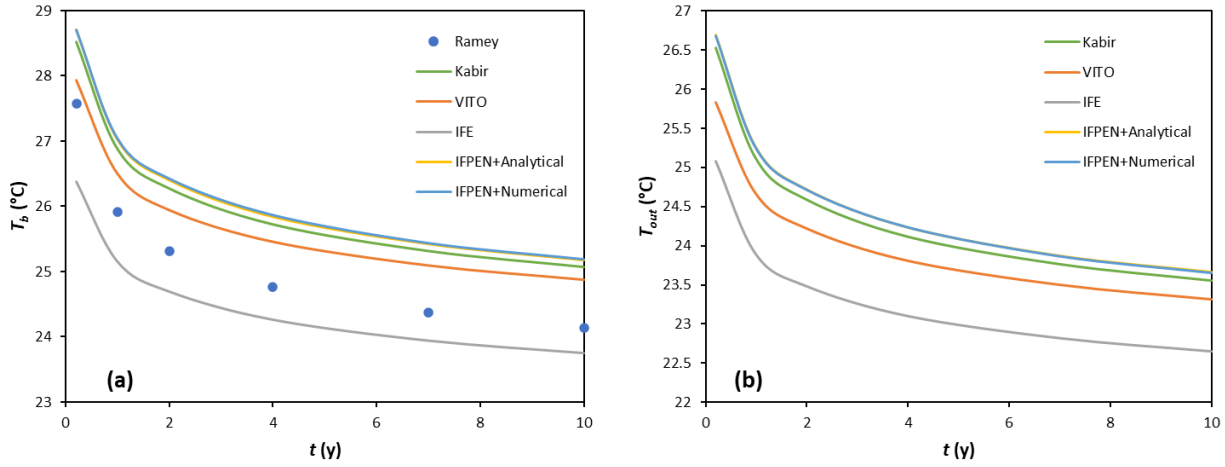

Figure 60. Comparison of the temporal evolution of (a) the temperature at the bottom of the annulus part and (b) the outlet temperature of the well for case e4.

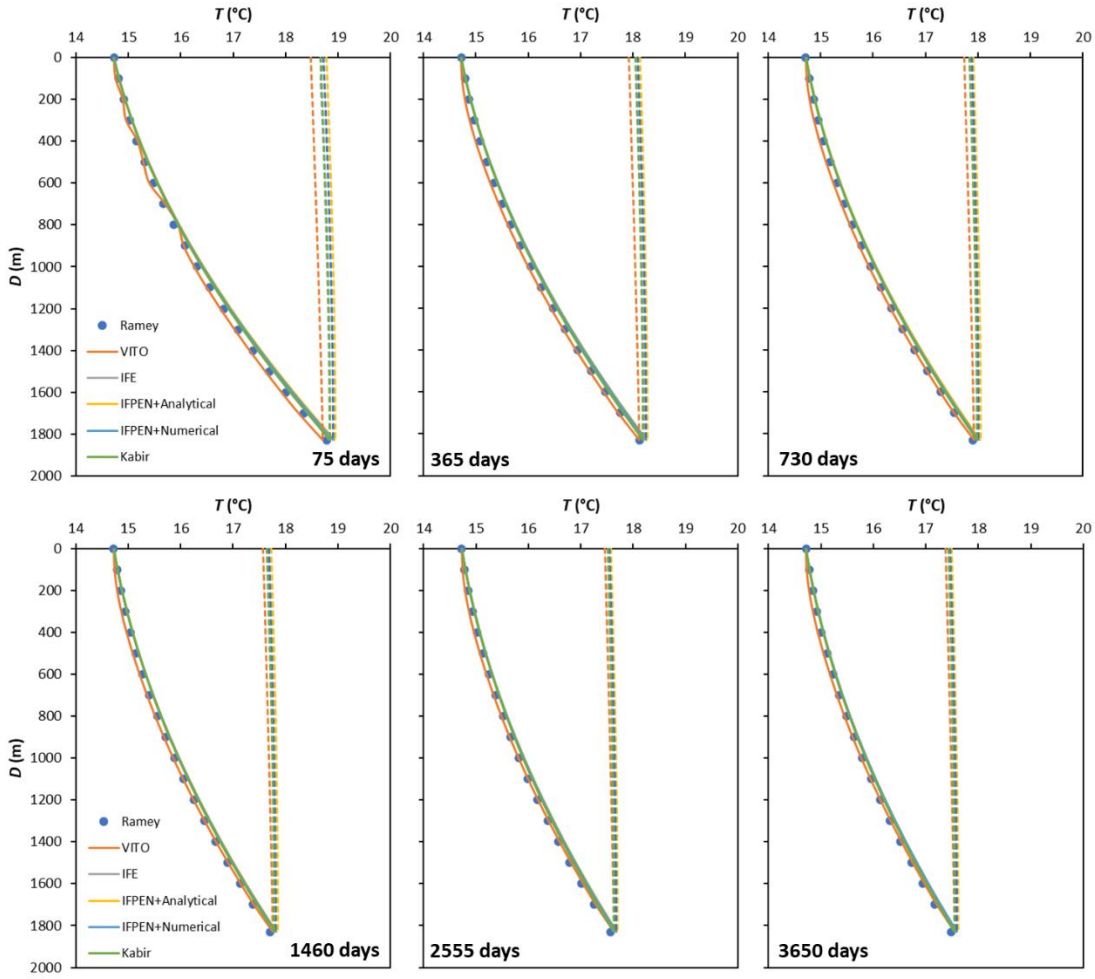

Figure 61. Comparison of fluid temperature along the well for case e5 at different times.

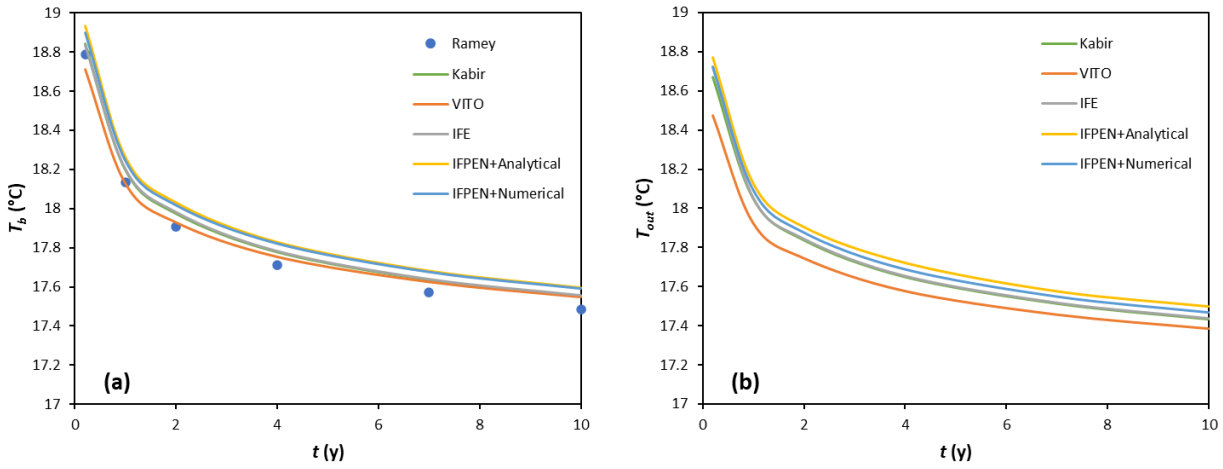

Figure 62. Comparison of the temporal evolution of (a) the temperature at the bottom of the annulus part and (b) the outlet temperature of the well for case e5.

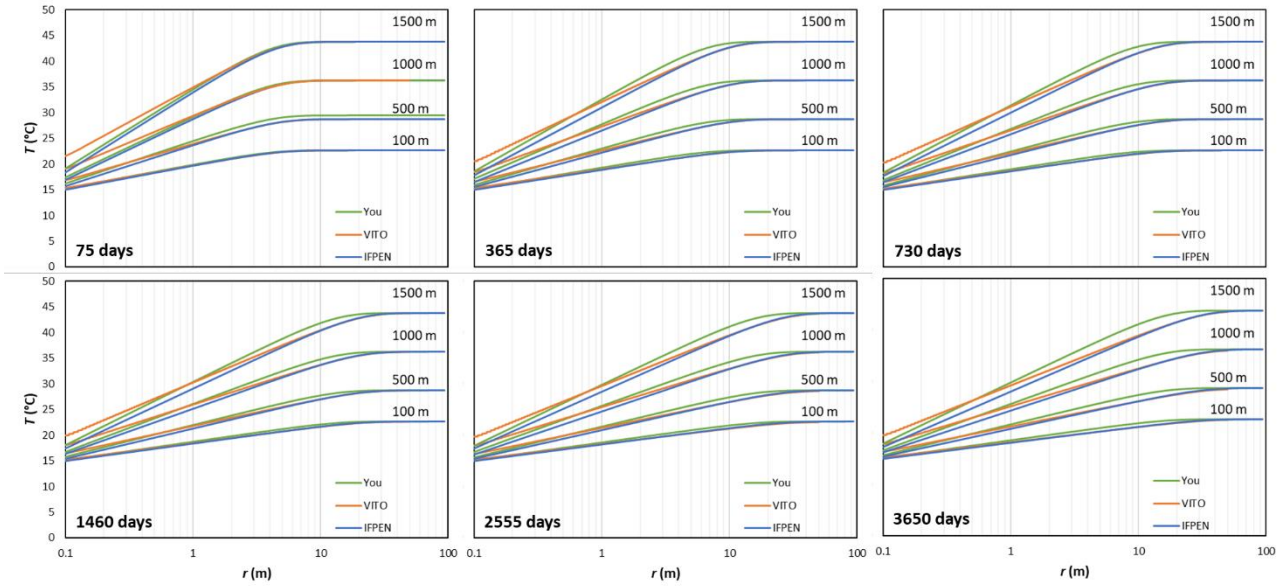

Figure 63. Comparison of temperature profiles in the formation at various depths and times for case e5 between GWellFM (IFPEN), COMSOL (VITO) and You's analytical model.